

Electroactive Polymer Composites - Analysis and Simulation

**Thesis submitted in partial fulfillment of the requirements for the degree of
“DOCTOR OF PHILOSOPHY”**

by

Limor

Tevet-Deree

Submitted to the Senate of Ben-Gurion University of the Negev

January 2008

Beer-Sheva

Electroactive Polymer Composites - Analysis and Simulation

**Thesis submitted in partial fulfillment of the requirements for the degree of
“DOCTOR OF PHILOSOPHY”**

by

Limor

Tevet-Deree

Submitted to the Senate of Ben-Gurion University of the Negev

Approved by the advisor _____

Approved by the Dean of the Kreitman School of Advanced Graduate Studies _____

January 2008

Beer-Sheva

This work was carried out under the supervision of

Professor Gal deBotton

In the Department of Mechanical Engineering

The Faculty of Engineering Science

ABSTRACT

The electromechanical coupling in electroactive polymer composites is studied. A general framework for characterizing the behavior of heterogeneous elastic dielectrics undergoing large deformations due to nonlinear electrostatic excitation is developed. The governing equations of the coupled electromechanical problem are obtained together with the appropriate boundary and interface continuity conditions.

In the limit of infinitesimal deformation theory of elasticity, a systematic representation of this coupling in terms of a macroscopic Maxwell stress is developed. This involves a fourth-order electromechanical tensor that depends on the concentration tensors relating the average electric and strain fields to their corresponding counterparts in the individual phases. The concentration tensors, which are determined from the uncoupled electrostatic and mechanical problems, can be extracted from available solutions and estimates.

In addition, a numerical tool to provide a solution for the electromechanical response of heterogeneous hyperelastic dielectrics is developed. The numerical calculations are based on finite element simulations by application of iterative procedure in the commercial code ABAQUS.

Exact results and estimates for various classes of composites are determined, and compared with corresponding finite element simulations of periodic composites with hexagonal unit cell. The marked dependency of the electromechanical coupling on the microstructure is highlighted with the aid of numerical examples. It is demonstrated that an improvement in the overall actuation strain can be achieved with appropriate spatial arrangement of the phases. Thus, for example the electromechanical coupling response of a soft dielectric matrix can be enhanced more than 65 times by adding 30% conductive oligomer particles. In particular,

it has been shown that the overall response of a composite actuator can be better than the responses of its constituents. Particularly, the actuation strain of composites whose phases have similar coupled strain response can be dramatically increased by increasing the contrast between the moduli of the phases.

Keywords: Active materials, Electroactive polymers (EAP), Electrostatics, Electro-mechanical coupling, Finite Elasticity, Composites, Homogenization.

CONTENTS

1. Introduction	1
2. Theory	5
2.1 Kinematics	5
2.2 Electric field	6
2.3 Rate of Dissipation of the system	10
2.3.1 Rate of external working	10
2.3.2 Total energy of the system	10
2.3.3 Rate of change of total energy	11
2.3.4 Rate of change of field energy	12
2.3.5 Rate of dissipation: the final expression	14
2.4 Governing equations	15
3. Applications to EAPCs	16
3.1 Heterogeneous hyperelastic dielectric	19
3.1.1 Solution for hyperelastic laminated EAPCs	20
3.1.2 Examples	23
3.2 The limit of small deformations elasticity	26
3.3 Applications to specific composite classes	31
3.3.1 Sequentially laminated composites	32
3.3.2 Hashin-Shtrikman estimates	34
3.3.3 Third order estimates	39
3.3.4 Periodic composites with hexagonal unit cell	41
3.3.5 A “naive” estimate	42
3.3.6 Examples	43

3.4 Optimization	50
3.4.1 Rank-2 laminated composites	51
3.4.2 Composites with fibers with elliptic cross section	53
4. FEM solver for EAPCs	58
4.1 The iterative procedure	59
4.2 Plane-strain simulation	61
4.3 Application to hexagonal unit cell	62
4.4 Naive estimate	65
4.5 Examples	66
5. Concluding remarks	70
 <i>Appendix</i>	 72
<i>A. Walpole's notation</i>	<i>73</i>
<i>B. Analytic solution for a homogeneous body</i>	<i>76</i>
<i>Bibliography</i>	<i>78</i>

LIST OF FIGURES

1.1	Grand challenge for the development of EAP actuated robotics . . .	2
2.1	Heterogeneous dielectric solid in an external field generated by thin electrodes with fixed potential	6
2.2	Heterogeneous electroactive polymer between two flat and thin electrodes	8
3.1	Rank-1 and rank-2 laminated composites	20
3.2	Actuation strain of a laminated EAPC as a function of the electric excitation field	23
3.3	Actuation strain of a laminated EAPC with phases whose electrostatic strain responses are identical	25
3.4	Schematic drawing of fiber with elliptic cross-section.	37
3.5	Effective properties of incompressible dielectric composites with hexagonal unit cell	42
3.6	Maxwell stresses as functions of the electric excitation field	43
3.7	Maxwell stresses as functions of the inclusions' volume fraction . . .	44
3.8	Maxwell stresses as functions of the the phases' dielectric contrast .	46
3.9	Actuation strains as functions of the electric excitation field	47
3.10	Actuation strains of rank-2 laminated composites as functions of the direction of the applied electric field	48
3.11	Actuation strains as functions of the contrast between the moduli of the phases	49
3.12	Normalized longitudinal strains of rank-2 laminated composites as functions of the applied electric field direction	50

3.13	Normalized longitudinal strains of rank-2 laminated composites as functions of the applied electric field direction	52
3.14	Normalized longitudinal strains of optimal rank-2 laminated composites as functions of the contrast between the moduli of the phases	54
3.15	Normalized longitudinal strains of composites with fibers with elliptic cross section as functions of the direction of the applied electric field	55
3.16	Normalized longitudinal strains of composites with fibers with elliptic cross section as functions of the applied electric field direction .	56
3.17	Normalized longitudinal strains of composites with fibers with elliptic cross section as functions of the inclusions' aspect ratio	57
4.1	Deformation of a medium with initial stresses.	60
4.2	Schematic iterative procedure of a medium with "post-stresses". . .	62
4.3	Schematic representation of the steps followed by the iterative procedure	63
4.4	Hexagonal unit cell	64
4.5	Longitudinal strains as functions of the excitation electric field . . .	66
4.6	Longitudinal strains as functions of the inclusions' volume fraction .	67
4.7	Longitudinal strains as functions of the phases' contrast.	68
4.8	Longitudinal strains as functions of the excitation electric field . . .	69

NOMENCLATURE

Symbol	Units	Description
A	m/m	Deformation Gradient
E	V/m	Electric Field
D	C/m ²	Electric Displacement Field
k		Dielectric Tensor
L	Pa	Elasticity Tensor
p	C/m ²	Polarization
<i>p</i>	Pa	Pressure
<i>q</i>	C/m ²	Surface Charge Density
T	Pa	Cauchy Stress Tensor
T_M	Pa	Maxwell Stress Tensor
t	Pa	Traction
u	m	Displacement Field
v	Pa	Particle Velocity
x	m	Material Point
y	m	Deformation
λ		Volume Fraction
ϵ_0	F/m ¹	Dielectric Constant of the Vacuum
ϵ		Infinitesimal Strain Tensor
ϕ	V	Electric Potential
μ	Pa	Shear Modulus
Σ	Pa	Nominal Stress Tensor
σ	Pa	Total Stress Tensor
θ	rad	Angle
χ		Susceptibility Tensor

¹ [F] = [C/V]

1. INTRODUCTION

Electroactive polymers (EAP) are polymers that can change their shape in response to electrical stimulation. These light weight and flexible materials can be used in a wide variety of applications such as robotic manipulators and vehicles, active damping and conformal control surfaces. Moreover, these actuators can be miniaturized and incorporated into MEMS and NEMS devices through the use of soft lithography. Significant progress in this field that was accomplished during the last decade has made these type of actuators feasible. In comparison with other types of active materials such as EAC (electroactive ceramics) and SMA (shape memory alloys), EAPs can undergo large strains, their response time is shorter their density is lower and their resilience is greater. In soft polymers these benefits can be used to construct actuators with large actuation ($> 50\%$) that appear to act similarly to biological muscles (Bar-Cohen, 2001). This attractive characteristic earned these polymers the name “artificial muscles”. In recent years the worldwide community of EAP expert are planning to develop a robotic arm that can be actuated by these polymers (Fig. 1.1). Progress towards this goal will lead to great benefits, particularly in the medical area, including effective prosthetics (Bar-Cohen, 2002).

The electromechanical coupling effect exists in all dielectric materials. The electromechanical coupling can be linear like in piezoelectric materials, or non-linear like in electrostatic and electrostrictive polymers. Thus, the piezoelectric effect is an electromechanical phenomenon in which the mechanical strains and stresses are coupled with the electric field and displacement linearly (Benveniste, 1993). On the other hand, the electrostrictive effect corresponds to a quadratic dependency of the strains or stresses on the electric polarization (Pelrine et al., 1998; Zhang and Scheinbeim, 2001). In some cases the electrostrictor is used as



Fig. 1.1: Grand challenge for the development of EAP actuated robotics (from Bar-Cohen, 2001).

an actuator, exploiting the nonlinear coupling. Nonetheless, these materials also exhibit a converse effect where the electrostatic fields depend on the mechanical fields (Sundar and Newnham, 1992). The electrostatic coupling results in a similar type of quadratic coupling (Bhattacharya et al., 2001). This however is a universal coupling effect due to the forces that develop in any dielectric subjected to electrostatic excitation (Tiersten, 1990). In general, it is not possible to distinguish between the electrostriction and the electrostatic coupling (McMeeking and Landis, 2005), nonetheless, in this work we consider a broad class of materials in which the electrostrictive effects are negligible and focus on the universal electrostatic coupling.

The coupled electromechanical analysis of materials undergoing large deformations must be executed within the framework of finite deformation elasticity. In pioneering works Toupin (1956) and Eringen (1963) developed a theoretical framework for dealing with the response of homogeneous elastic dielectric materials. More recently, McMeeking and Landis (2005); Dorfmann and Ogden (2005); Gei and Magnarelli (2006) and Bustamante et al. (2008) among others, considered fundamental theoretical aspects related to the coupling phenomena in active elastomers.

We recall that a severe limitation on the usage of these polymers as electro-

mechanical actuators results from the low actuation force and the large electric field ($\sim 100[\text{V}/\mu\text{m}]$) required for meaningful actuation. The reason is the poor electro-mechanical coupling in typical polymers: this in turn arises from the fact that the typical polymers have a limited ratio of dielectric to elastic modulus (flexible polymers have low dielectric modulus while high dielectric moduli polymers are stiff). However, recent experimental works suggest that this limitation may be overcome by making *electroactive polymer composites* (EAPCs) of flexible and high dielectric modulus materials (Zhang et al., 2002; Huang et al., 2004). In their work Huang et al. described a three-phase polymer based actuator with more than 8% actuation strain which is attained with an activation field of $20[\text{V}/\mu\text{m}]$. The enhanced coupling is achieved in the heterogeneous media thanks to the fluctuations in the electric field. These fluctuations, and hence also the electromechanical coupling, depend extremely sensitively on the microstructure. One approach to tackle this problem is by fitting appropriate phenomenological models (*e.g.*, Kankanala and Triantafyllidis, 2004; Landis, 2004). A different path was considered by deBotton et al. (2007) who determined the response of these composites by application of homogenization approach.

In this work we develop a general framework for characterizing the behavior of EAPCs undergoing large actuation strains. The governing equations together with the required statements of the boundary and the interface continuity conditions for the coupled electromechanical problem in the heterogeneous elastic dielectric are obtained. Applying this variational principle we derive explicit expressions for the actuation strains of rank-1 laminated composites made out of two incompressible neo-Hookean dielectric phases.

As a first step toward the understanding of the role of the microstructure in the nonlinear coupling phenomenon, the rest of the analysis in this work will be carried out within the limit of infinitesimal deformation theory of elasticity. Furthermore, in electromechanical actuators a state where the electrostatic and the mechanical energies are of the same order is assumed. Alternatively, we may consider a state where the stresses (elastic and electrostatic induced stress) are of

the same order (McMeeking and Landis, 2005). This, for example, may occur when a large excitation field is applied on electronic devices like capacitors, made out of ceramics with high dielectric constant. We recall that some ceramics have dielectric constants of more than 1000 (Uchino and Leslie, 1980), and if the excitation field is $50[\text{V}/\mu\text{m}]$, the induced electrostatic stress is about $25[\text{MPa}]$. In these cases the level of the stresses is not negligible. However, since the strains are small, an analysis within the framework of infinitesimal deformation elasticity is justified.

We provide a general method for determining the overall or effective electro-mechanical coupling response by generalizing the work of Levin (1967) for the effective thermoelastic coupling of composites. By application of this procedure exact expressions for the response of sequentially laminated composites, estimates of the Hashin-Shtrikman type, and higher order estimates for composites with arbitrary microstructures are determined. For comparison, finite element (FE) simulations of periodic composites with hexagonal unit cell are carried out too. The numerical simulations are executed with the aid of an external procedure coupled with the commercial FE code ABAQUS.

Next, the analytic expressions for anisotropic composites such as rank-2 laminated composites and composites with fibers with elliptic cross section are used to reveal the best possible microstructure that provide maximal actuation under given boundary conditions.

Finally, the FE solver is expanded to deal with the electromechanical coupling response of heterogeneous hyperelastic dielectrics undergoing large deformations. By application of the numerical procedure we simulate the overall actuation of various periodic composites with hexagonal unit cell made out of two incompressible neo-Hookean dielectric phases.

2. THEORY

In this Chapter we examine the general variational principle characterizing the behavior of elastic dielectric solids under the combined mechanical and electrical loads. We follow the Ph.D. thesis of Xiao (2004) where the corresponding variational principle was derived for a homogeneous dielectric with charge sources, and formulate it to the case of heterogeneous solids. This fundamental study provides the tools to identify the appropriate transformation from the microscopic level to the macroscopic level (*e.g.*, Hill and Rice, 1973, for the corresponding purely mechanical case). We note that while writing this work the Ph.D. thesis of Xiao (2004) was available, although recently, a paper based on that work was published (Xiao and Bhattacharya, 2008).

We present a comprehensive continuum model that treats elastic dielectric composite materials as deformable and polarizable solids. Polarizable means that the material may be spontaneously polarized. Following arguments similar to those of Coleman and Noll (1963) and Xiao (2004) we use the dissipation inequality (second law of thermodynamics) to write down the governing equations with polarization, electric potential and elastic deformation as variables.

2.1 Kinematics

Consider a n -phase EAPC in an external electric field generated by thin electrodes with fixed potential (Fig. 2.1). The electrodes are attached on a portion S_v of the composite's boundary and move with the composite. The composite occupies a volume region $\Omega \subset \mathbb{R}^3$, with boundary $\partial\Omega$, in the reference configuration. Each homogeneous phase in the composite occupies a volume $\Omega^{(r)}$ ($r = 1, 2, \dots, n$) and we define $\Omega^{(0)} = \mathbb{R}^3 \setminus \bigcup_{r=1}^n \Omega^{(r)}$. The region of the r -phase in the current

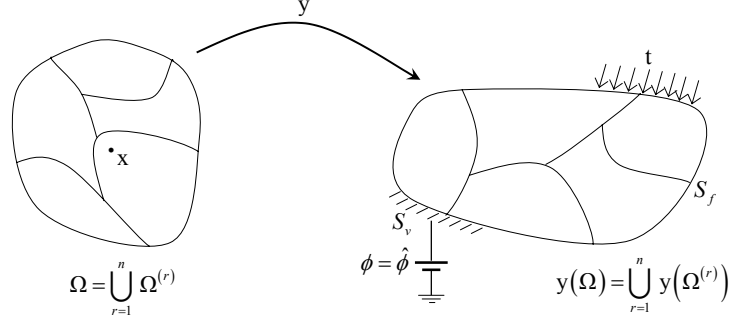


Fig. 2.1: Heterogeneous dielectric solid in an external field generated by thin electrodes with fixed potential.

configuration is $\mathbf{y}(\Omega^{(r)}) = B^{(r)}$ and we note that $B^{(0)} = \mathbf{y}(\Omega^{(0)})$ is the external domain out of the composite. We also denote by ∂B the boundary of the composite which separates between $B = \bigcup_{r=1}^n B^{(r)}$ and $B^{(0)}$. The deformation gradient is $\mathbf{A} = \nabla_{\mathbf{x}}\mathbf{y}$, and we assume that the deformation is invertible and $J^{(r)} = \det(\mathbf{A}^{(r)}) > 0$. We emphasize that while the deformation \mathbf{y} is continuous, the deformation gradient is continuous in each phase but not in \mathbb{R}^3 .

2.2 Electric field

The polarization in the dielectric phases as well as the charges on the surfaces of the electrodes generate an electric field in all space. The electrostatic potential ϕ is continuous, and at any point in each dielectric phase ($r = 1, 2, \dots, n$) is obtained by solving Maxwell equation:

$$\nabla_{\mathbf{y}} \cdot [\epsilon_0 \mathbf{E}^{(r)} + \mathbf{p}^{(r)} \chi(B^{(r)})] = 0, \quad (2.1)$$

subjected to

$$\phi = \hat{\phi} \quad \text{on } S_v,$$

$$\phi \rightarrow 0 \quad \text{as } |\mathbf{y}| \rightarrow \infty,$$

where ϵ_0 is the dielectric constant of the vacuum, $\mathbf{E} = -\nabla_{\mathbf{y}}\phi$ is the electric field, \mathbf{p} is the polarization per unit deformed volume, and where we assume that there

is no distribution of charge sources in the dielectric phases. Here the characteristic function $\chi(B^{(r)})$ of domain $B^{(r)}$ is such that $\chi = 1$ if \mathbf{y} is inside domain $B^{(r)}$ and $\chi = 0$ otherwise. We note that

$$\mathbf{D} \equiv \epsilon_0 \mathbf{E} + \mathbf{p} \quad (2.2)$$

is the electric displacement field. Following Toupin (1956), we define the polarization per unit undeformed volume via the relation

$$\mathbf{p}_0^{(r)}(\mathbf{x}) = J^{(r)} \mathbf{p}^{(r)}(\mathbf{y}(\mathbf{x})). \quad (2.3)$$

A weak form of Maxwell equation in \mathbb{R}^3 can be written in the form

$$-\sum_{r=0}^n \int_{B^{(r)}} [\epsilon_0 \mathbf{E}^{(r)} + \mathbf{p}^{(r)}] \cdot \nabla_{\mathbf{y}} \psi \, dv = \int_{S_v} q \psi \, ds, \quad (2.4)$$

$$\phi = \hat{\phi} \quad \text{on } S_v,$$

where ψ is continuous and differentiable, and q is the surface charge density on S_v .

In a heterogeneous solid the jump conditions across the interfaces must be appropriately treated. In a general setting the jump conditions across an interface between two phases may be described as follows. Consider a point on an interface charged with q (Fig. 2.2). The jump across the interface between phases r and s is defined as

$$[[\xi]] = \xi^{(s)} - \xi^{(r)}, \quad (2.5)$$

with ξ being some variable defined in both phases. $\hat{\mathbf{n}}$ is a unit normal of the interface pointing from phase s to r . In the sequel, for convenience we always take $\hat{\mathbf{n}}$ to point from the phase with a higher index to the one with a lower index. Thus, in definition (2.5) we have that $s > r$.

Let $\hat{\mathbf{y}}(\alpha)$ be a curve on the interface at time t_0 parameterized by α . From the continuity of ϕ

$$\phi^{(r)}(\hat{\mathbf{y}}(\alpha)) = \phi^{(s)}(\hat{\mathbf{y}}(\alpha)). \quad (2.6)$$

Differentiating it with respect to α

$$[[\nabla_{\mathbf{y}} \phi]] \cdot \frac{\partial \hat{\mathbf{y}}}{\partial \alpha} = 0. \quad (2.7)$$

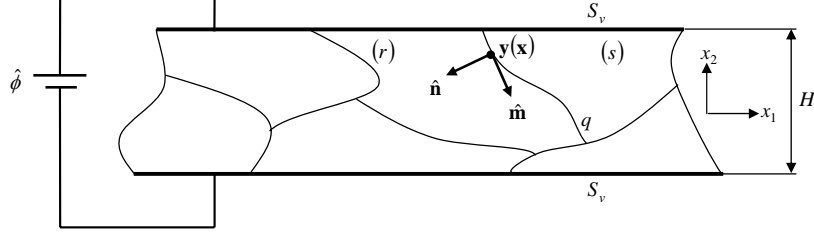


Fig. 2.2: Heterogeneous electroactive polymer between two flat and thin electrodes.

Remembering that this holds for any curve on the interface, the following continuity condition on \mathbf{E} is obtained

$$[[\mathbf{E}]] \cdot \hat{\mathbf{m}} = 0, \quad \forall \hat{\mathbf{n}} \cdot \hat{\mathbf{m}} = 0. \quad (2.8)$$

Hence, the jump in the electric field is

$$[[\mathbf{E}]] = ([[\mathbf{E}]]) \cdot \hat{\mathbf{n}}. \quad (2.9)$$

The jump in the electric displacement field across the interface is

$$[[\mathbf{D}]] \cdot \hat{\mathbf{n}} = -q. \quad (2.10)$$

Assume that the interface does not propagate in the reference configuration, therefore, the particle velocity remains continuous across the interface. Then, from the continuity of the electric potential ϕ across the interface

$$\phi^{(r)}(\mathbf{y}(\mathbf{x}, t), t) = \phi^{(s)}(\mathbf{y}(\mathbf{x}, t), t), \quad (2.11)$$

so

$$\overline{\dot{\phi}^{(r)}(\mathbf{y}(\mathbf{x}, t), t)} = \overline{\dot{\phi}^{(s)}(\mathbf{y}(\mathbf{x}, t), t)}, \quad (2.12)$$

thus,

$$\overset{\circ}{\phi}^{(r)} + \nabla_{\mathbf{y}}^{(r)} \phi \cdot \mathbf{v} = \overset{\circ}{\phi}^{(s)} + \nabla_{\mathbf{y}}^{(s)} \phi \cdot \mathbf{v}, \quad (2.13)$$

or alternatively,

$$\overset{\circ}{\phi}^{(r)} - \mathbf{E}^{(r)} \cdot \mathbf{v} = \overset{\circ}{\phi}^{(s)} - \mathbf{E}^{(s)} \cdot \mathbf{v}. \quad (2.14)$$

We point out that $\overset{\circ}{\phi}$ and $\dot{\phi}$ denote the material time derivative and the spatial time derivative of ϕ , respectively. From Eq. (2.14) we have

$$[[\overset{\circ}{\phi}]] = [[\mathbf{E}]] \cdot \mathbf{v}, \quad (2.15)$$

where \mathbf{v} , the particle velocity of the material point \mathbf{x} , is continuous across the interface. For latter use we note that when $\phi = \hat{\phi}$ is constant

$$\langle \dot{\phi} \rangle = \langle \mathbf{E} \rangle \cdot \mathbf{v}, \quad (2.16)$$

where

$$\langle \xi \rangle = \frac{\xi^{(r)} + \xi^{(s)}}{2}$$

is the average of the limiting values of the quantity ξ .

For later utilization, we present the important quantity of *Maxwell stress tensor* (e.g., Tiersten, 1990)

$$\mathbf{T}_M = \mathbf{E} \otimes \mathbf{D} - \frac{\epsilon_0}{2} \mathbf{E} \cdot \mathbf{E} \mathbf{I}. \quad (2.17)$$

The divergence of \mathbf{T}_M can be specify as

$$\begin{aligned} \nabla_{\mathbf{y}} \cdot \mathbf{T}_M &= \nabla_{\mathbf{y}} \cdot \left(\mathbf{E} \otimes \mathbf{D} - \frac{\epsilon_0}{2} \mathbf{E} \cdot \mathbf{E} \mathbf{I} \right) \\ &= (\nabla_{\mathbf{y}} \mathbf{E}) \cdot \mathbf{D} + \mathbf{E} (\nabla_{\mathbf{y}} \cdot \mathbf{D}) - \epsilon_0 (\nabla_{\mathbf{y}} \mathbf{E}) \cdot \mathbf{E} \\ &= (\nabla_{\mathbf{y}} \mathbf{E}) \cdot \mathbf{p}. \end{aligned} \quad (2.18)$$

In the third equality, since $\mathbf{E} = -\nabla_{\mathbf{y}} \phi$ we make use of the fact that $\nabla_{\mathbf{y}} \mathbf{E} = (\nabla_{\mathbf{y}} \mathbf{E})^T$, and whenever the volumetric charge density vanishes it follows from Maxwell equation that $\nabla_{\mathbf{y}} \cdot \mathbf{D} = 0$. In the following we make use of the identity

$$[[\phi \psi]] = [[\phi]] \langle \psi \rangle + [[\psi]] \langle \phi \rangle. \quad (2.19)$$

The jump condition on \mathbf{T}_M is derived from the discontinuities of \mathbf{E} and \mathbf{D} across the interface

$$\begin{aligned} [[\mathbf{T}_M \hat{\mathbf{n}}]] &= \left[\left(\mathbf{E} \otimes \mathbf{D} - \frac{\epsilon_0}{2} \mathbf{E} \cdot \mathbf{E} \mathbf{I} \right) \hat{\mathbf{n}} \right] \\ &= [[\mathbf{E}]] \langle \mathbf{D} \cdot \hat{\mathbf{n}} \rangle + \langle \mathbf{E} \rangle [[\mathbf{D} \cdot \hat{\mathbf{n}}]] - \epsilon_0 \langle \mathbf{E} \rangle \cdot [[\mathbf{E}]] \hat{\mathbf{n}} \\ &= [[\mathbf{E}]] (\epsilon_0 \langle \mathbf{E} \rangle \cdot \hat{\mathbf{n}} + \langle \mathbf{p} \rangle \cdot \hat{\mathbf{n}}) + \langle \mathbf{E} \rangle [[\mathbf{D}]] \cdot \hat{\mathbf{n}} - \epsilon_0 \langle \mathbf{E} \rangle \cdot [[\mathbf{E}]] \hat{\mathbf{n}} \\ &= \epsilon_0 ([[\mathbf{E}]]) \cdot \hat{\mathbf{n}} (\langle \mathbf{E} \rangle \cdot \hat{\mathbf{n}}) \hat{\mathbf{n}} + ([[\mathbf{E}]]) \cdot \hat{\mathbf{n}} (\langle \mathbf{p} \rangle \cdot \hat{\mathbf{n}}) \hat{\mathbf{n}} \\ &\quad + \langle \mathbf{E} \rangle [[\mathbf{D}]] \cdot \hat{\mathbf{n}} - \epsilon_0 ([[\mathbf{E}]]) \cdot \hat{\mathbf{n}} (\langle \mathbf{E} \rangle \cdot \hat{\mathbf{n}}) \hat{\mathbf{n}} \\ &= ([[\mathbf{E}]]) \cdot \hat{\mathbf{n}} (\langle \mathbf{p} \rangle \cdot \hat{\mathbf{n}}) \hat{\mathbf{n}} + \langle \mathbf{E} \rangle [[\mathbf{D} \cdot \hat{\mathbf{n}}]] \\ &= ([[\mathbf{E}]]) \cdot \hat{\mathbf{n}} (\langle \mathbf{p} \rangle \cdot \hat{\mathbf{n}}) \hat{\mathbf{n}} - q \langle \mathbf{E} \rangle. \end{aligned} \quad (2.20)$$

If the interface is charge free then the last term vanishes and

$$\llbracket \mathbf{T}_M \hat{\mathbf{n}} \rrbracket = \llbracket \mathbf{E} \cdot \hat{\mathbf{n}} \rrbracket \langle \mathbf{p} \cdot \hat{\mathbf{n}} \rangle \hat{\mathbf{n}}. \quad (2.21)$$

If, on the other hand, $\phi = \hat{\phi}$ is constant on the interface, by making use of the second equality in Eq. (2.20), Eqs. (2.15)-(2.16) and expression (2.19)

$$\begin{aligned} \llbracket \mathbf{T}_M \hat{\mathbf{n}} \rrbracket \cdot \mathbf{v} &= \left[\left[\overset{\circ}{\phi} \right] \right] \langle \mathbf{D} \rangle \cdot \hat{\mathbf{n}} + \left\langle \overset{\circ}{\phi} \right\rangle \llbracket \mathbf{D} \rrbracket \cdot \hat{\mathbf{n}} - \epsilon_0 \langle \mathbf{E} \rangle \cdot \llbracket \mathbf{E} \rrbracket (\mathbf{v} \cdot \hat{\mathbf{n}}) \\ &= \left[\left[\overset{\circ}{\phi} \mathbf{D} \right] \right] \cdot \hat{\mathbf{n}} - \frac{\epsilon_0}{2} \left[\left[|E|^2 \right] \right] (\mathbf{v} \cdot \hat{\mathbf{n}}). \end{aligned} \quad (2.22)$$

2.3 Rate of Dissipation of the system

The rate of dissipation of the whole system \mathcal{D} is defined as the difference between the rate of external working \mathcal{F} and the rate of the change of the total energy $d\mathcal{E}/dt$

$$\mathcal{D} = \mathcal{F} - \frac{d\mathcal{E}}{dt}. \quad (2.23)$$

2.3.1 Rate of external working

The rate of external working \mathcal{F} includes the electric work done by the electrodes and the mechanical work done by external forces

$$\mathcal{F} = \hat{\phi} \frac{d}{dt} \int_{S_v} q ds + \int_{\mathbf{y}(\partial_s \Omega)} \mathbf{t} \cdot \mathbf{v} ds. \quad (2.24)$$

We assume that external forces are acting only on the boundaries of the EAPC. Hence, we rewrite Eq. (2.24) as

$$\mathcal{F} = \hat{\phi} \frac{d}{dt} \int_{S_v} q ds + \sum_{r=1}^n \int_{\partial B^{(r)} \cap \partial B^{(0)}} \mathbf{t} \cdot \mathbf{v} ds. \quad (2.25)$$

2.3.2 Total energy of the system

The total energy of the system consists of (1) the energy stored in the heterogeneous body and (2) the electrostatic field energy generated by external and internal sources

$$\mathcal{E} = \sum_{r=1}^n \int_{\Omega^{(r)}} W^{(r)} dV + \frac{\epsilon_0}{2} \sum_{r=0}^n \int_{B^{(r)}} |\mathbf{E}^{(r)}|^2 dv. \quad (2.26)$$

Here, $W^{(r)}$ is the stored energy per unit reference volume in the phase r , and we assume that in each phase it depends on the polarization and the deformation gradient *i.e.*,

$$W^{(r)} = W^{(r)} \left(\mathbf{p}_0^{(r)}, \mathbf{A}^{(r)} \right). \quad (2.27)$$

2.3.3 Rate of change of total energy

The rate of change of the total energy $d\mathcal{E}/dt$ is,

$$\frac{d\mathcal{E}}{dt} = \sum_{r=1}^n \int_{\Omega^{(r)}} \dot{W}_0^{(r)} dV + \frac{d}{dt} \left[\frac{1}{2} \sum_{r=0}^n \int_{B^{(r)}} \epsilon_0 |\mathbf{E}^{(r)}|^2 dv \right]. \quad (2.28)$$

The first term on the right-hand side of Eq. (2.28) is

$$\sum_{r=1}^n \int_{\Omega^{(r)}} \dot{W}_0^{(r)} \left(\mathbf{p}_0^{(r)}, \mathbf{A}^{(r)} \right) dV = \sum_{r=1}^n \int_{\Omega^{(r)}} \frac{\partial W^{(r)}}{\partial \mathbf{p}_0} \cdot \dot{\mathbf{p}}_0^{(r)} dV + \sum_{r=1}^n \int_{\Omega^{(r)}} \frac{\partial W^{(r)}}{\partial \mathbf{A}} : \dot{\mathbf{A}}^{(r)} dV. \quad (2.29)$$

By using the relation (*e.g.*, Ogden, 1997)

$$\frac{\partial W}{\partial \mathbf{A}} : \dot{\mathbf{A}} = J \mathbf{T} : \nabla_{\mathbf{y}} \mathbf{v}, \quad (2.30)$$

where \mathbf{T} is the Cauchy stress tensor, we can simplify the second term in Eq. (2.29)

$$\begin{aligned} & \sum_{r=1}^n \int_{\Omega^{(r)}} \frac{\partial W^{(r)}}{\partial \mathbf{A}} : \dot{\mathbf{A}}^{(r)} dV \\ &= \sum_{r=1}^n \int_{B^{(r)}} \mathbf{T}^{(r)} : \nabla_{\mathbf{y}} \mathbf{v} dv \\ &= \sum_{r=1}^n \int_{B^{(r)}} \nabla_{\mathbf{y}} \cdot (\mathbf{T}^{(r)} \mathbf{v}) dv - \sum_{r=1}^n \int_{B^{(r)}} (\nabla_{\mathbf{y}} \cdot \mathbf{T}^{(r)}) \cdot \mathbf{v} dv \\ &= \sum_{r=1}^n \int_{\partial B^{(r)}} (\mathbf{T}^{(r)} \hat{\mathbf{n}}) \cdot \mathbf{v} ds - \sum_{r=1}^n \int_{B^{(r)}} (\nabla_{\mathbf{y}} \cdot \mathbf{T}^{(r)}) \cdot \mathbf{v} dv \\ &= \sum_{r=0}^{n-1} \sum_{s=r+1}^n \int_{\partial B^{(r)} \cap \partial B^{(s)}} [\mathbf{T} \hat{\mathbf{n}}] \cdot \mathbf{v} ds - \sum_{r=1}^n \int_{B^{(r)}} (\nabla_{\mathbf{y}} \cdot \mathbf{T}^{(r)}) \cdot \mathbf{v} dv. \end{aligned} \quad (2.31)$$

In the last equality of Eq. (2.31) we make use of the fact that in $B^{(0)}$, $\mathbf{T}^{(0)} \equiv 0$.

Finally,

$$\begin{aligned} & \sum_{r=1}^n \int_{\Omega^{(r)}} \dot{W}_0^{(r)} \left(\mathbf{p}_0^{(r)}, \mathbf{A}^{(r)} \right) dV = \sum_{r=1}^n \int_{\Omega^{(r)}} \frac{\partial W^{(r)}}{\partial \mathbf{p}_0} \cdot \dot{\mathbf{p}}_0^{(r)} dV \\ & + \sum_{r=0}^{n-1} \sum_{s=r+1}^n \int_{\partial B^{(r)} \cap \partial B^{(s)}} [\mathbf{T} \hat{\mathbf{n}}] \cdot \mathbf{v} ds - \sum_{r=1}^n \int_{B^{(r)}} (\nabla_{\mathbf{y}} \cdot \mathbf{T}^{(r)}) \cdot \mathbf{v} dv. \end{aligned} \quad (2.32)$$

2.3.4 Rate of change of field energy

First, we set $\psi = \phi$ in Eq. (2.4)

$$\sum_{r=0}^n \int_{B^{(r)}} \epsilon_0 \mathbf{E}^{(r)} \cdot \mathbf{E}^{(r)} dv = - \sum_{r=1}^n \int_{B^{(r)}} \mathbf{E}^{(r)} \cdot \mathbf{p}^{(r)} dv + \int_{S_v} \hat{\phi} q ds, \quad (2.33)$$

with the understanding that $\mathbf{p}^{(0)} \equiv 0$. Therefore,

$$\begin{aligned} \frac{d}{dt} \sum_{r=0}^n \int_{B^{(r)}} \epsilon_0 |\mathbf{E}^{(r)}|^2 dv &= - \frac{d}{dt} \sum_{r=1}^n \int_{B^{(r)}} \mathbf{E}^{(r)} \cdot \mathbf{p}^{(r)} dv + \hat{\phi} \frac{d}{dt} \int_{S_v} q ds \\ &= - \frac{d}{dt} \sum_{r=1}^n \int_{\Omega^{(r)}} \mathbf{E}^{(r)} \cdot \mathbf{p}_0^{(r)} dV + \hat{\phi} \frac{d}{dt} \int_{S_v} q ds \\ &= - \sum_{r=1}^n \int_{\Omega^{(r)}} \left[\frac{d}{dt} (\mathbf{E}^{(r)} \cdot \mathbf{p}_0^{(r)}) + \mathbf{E}^{(r)} \cdot \dot{\mathbf{p}}_0^{(r)} \right] dV + \hat{\phi} \frac{d}{dt} \int_{S_v} q ds \\ &= \sum_{r=1}^n \int_{\Omega^{(r)}} \left[(\nabla_{\mathbf{y}} \dot{\phi}^{(r)} - \nabla_{\mathbf{y}} \mathbf{E}^{(r)} \cdot \mathbf{v}) \cdot \mathbf{p}_0^{(r)} \right] dV \\ &\quad - \sum_{r=1}^n \int_{\Omega^{(r)}} \mathbf{E}^{(r)} \cdot \dot{\mathbf{p}}_0^{(r)} dV + \hat{\phi} \frac{d}{dt} \int_{S_v} q ds \\ &= \sum_{r=1}^n \int_{B^{(r)}} (\nabla_{\mathbf{y}} \dot{\phi}^{(r)} - \nabla_{\mathbf{y}} \mathbf{E}^{(r)} \cdot \mathbf{v}) \cdot \mathbf{p}^{(r)} dv \\ &\quad - \sum_{r=1}^n \int_{\Omega^{(r)}} \mathbf{E}^{(r)} \cdot \dot{\mathbf{p}}_0^{(r)} dV + \hat{\phi} \frac{d}{dt} \int_{S_v} q ds. \end{aligned} \quad (2.34)$$

By making use of Eq. (2.18) we finally get

$$\begin{aligned} \frac{d}{dt} \sum_{r=0}^n \int_{B^{(r)}} \epsilon_0 |\mathbf{E}^{(r)}|^2 dv &= \sum_{r=1}^n \int_{B^{(r)}} \nabla_{\mathbf{y}} \dot{\phi}^{(r)} \cdot \mathbf{p}^{(r)} dv - \sum_{r=1}^n \int_{B^{(r)}} (\nabla_{\mathbf{y}} \cdot \mathbf{T}_M^{(r)}) \cdot \mathbf{v} dv \\ &\quad - \sum_{r=1}^n \int_{\Omega^{(r)}} \mathbf{E}^{(r)} \cdot \dot{\mathbf{p}}_0^{(r)} dV + \hat{\phi} \frac{d}{dt} \int_{S_v} q ds. \end{aligned} \quad (2.35)$$

Second, we multiply $\dot{\phi}^{(r)}$ on both sides of Maxwell equation (2.1) and integrate over \mathbb{R}^3 to obtain

$$\begin{aligned} 0 &= \sum_{r=0}^n \int_{B^{(r)}} \nabla_{\mathbf{y}} \cdot (\epsilon_0 \mathbf{E}^{(r)} + \mathbf{p}^{(r)}) \dot{\phi}^{(r)} dv \\ &= - \sum_{r=0}^n \int_{B^{(r)}} \nabla_{\mathbf{y}} \dot{\phi}^{(r)} \cdot (\epsilon_0 \mathbf{E}^{(r)} + \mathbf{p}^{(r)}) dv + \sum_{r=0}^n \int_{\partial B^{(r)}} \dot{\phi}^{(r)} (\epsilon_0 \mathbf{E}^{(r)} + \mathbf{p}^{(r)}) \cdot \hat{\mathbf{n}} ds, \end{aligned} \quad (2.36)$$

The boundary term in Eq. (2.36) is

$$\begin{aligned} & \sum_{r=0}^{n-1} \sum_{s=r+1}^n \int_{\partial B^{(r)} \cap \partial B^{(s)}} \left[\dot{\phi}^{(s)} (\epsilon_0 \mathbf{E}^{(s)} + \mathbf{p}^{(s)}) - \dot{\phi}^{(r)} (\epsilon_0 \mathbf{E}^{(r)} + \mathbf{p}^{(r)}) \right] \cdot \hat{\mathbf{n}} \, ds \\ &= \sum_{r=0}^{n-1} \sum_{s=r+1}^n \int_{\partial B^{(r)} \cap \partial B^{(s)}} \left[\dot{\phi} \mathbf{D} \right] \cdot \hat{\mathbf{n}} \, ds, \end{aligned} \quad (2.37)$$

by noting that on the outer boundary of $B^{(0)}$ (*i.e.*, $\mathbf{y} \rightarrow \infty$) the integral vanishes.

Then we can rewrite Eq. (2.36) as

$$\begin{aligned} & \sum_{r=0}^n \int_{B^{(r)}} \epsilon_0 \nabla_{\mathbf{y}} \dot{\phi}^{(r)} \cdot \mathbf{E}^{(r)} \, dv \\ &= - \sum_{r=1}^n \int_{B^{(r)}} \nabla_{\mathbf{y}} \dot{\phi}^{(r)} \cdot \mathbf{p}^{(r)} \, dv + \sum_{r=0}^{n-1} \sum_{s=r+1}^n \int_{\partial B^{(r)} \cap \partial B^{(s)}} \left[\dot{\phi} \mathbf{D} \right] \cdot \hat{\mathbf{n}} \, ds, \end{aligned} \quad (2.38)$$

Next, by using Reynold's transport theorem

$$\begin{aligned} & \frac{d}{dt} \left[\frac{1}{2} \sum_{r=0}^n \int_{B^{(r)}} \epsilon_0 |\mathbf{E}^{(r)}|^2 \, dv \right] \\ &= \frac{\epsilon_0}{2} \sum_{r=0}^n \frac{d}{dt} \int_{B^{(r)}} |\mathbf{E}^{(r)}|^2 \, dv \\ &= \frac{\epsilon_0}{2} \sum_{r=0}^n \int_{B^{(r)}} \frac{\partial}{\partial t} |\mathbf{E}^{(r)}|^2 \, dv + \frac{\epsilon_0}{2} \sum_{r=0}^n \int_{\partial B^{(r)}} |\mathbf{E}^{(r)}|^2 (\mathbf{v} \cdot \hat{\mathbf{n}}) \, ds \\ &= - \sum_{r=0}^n \int_{B^{(r)}} \epsilon_0 \nabla_{\mathbf{y}} \dot{\phi}^{(r)} \cdot \mathbf{E}^{(r)} \, dv + \frac{\epsilon_0}{2} \sum_{r=0}^{n-1} \sum_{s=r+1}^n \int_{\partial B^{(r)} \cap \partial B^{(s)}} \left[|\mathbf{E}|^2 \right] (\mathbf{v} \cdot \hat{\mathbf{n}}) \, ds. \end{aligned} \quad (2.39)$$

Putting together Eq. (2.38) and Eq. (2.39), and by using expression (2.22)

$$\begin{aligned} \frac{d}{dt} \left[\frac{1}{2} \sum_{r=0}^n \int_{B^{(r)}} \epsilon_0 |\mathbf{E}^{(r)}|^2 \, dv \right] &= \sum_{r=1}^n \int_{B^{(r)}} \nabla_{\mathbf{y}} \dot{\phi}^{(r)} \cdot \mathbf{p}^{(r)} \, dv \\ &\quad - \sum_{r=0}^{n-1} \sum_{s=r+1}^n \int_{\partial B^{(r)} \cap \partial B^{(s)}} \left[\dot{\phi} \mathbf{D} \right] \cdot \hat{\mathbf{n}} \, ds \\ &\quad + \frac{\epsilon_0}{2} \sum_{r=0}^{n-1} \sum_{s=r+1}^n \int_{\partial B^{(r)} \cap \partial B^{(s)}} \left[|\mathbf{E}|^2 \right] (\mathbf{v} \cdot \hat{\mathbf{n}}) \, ds \quad (2.40) \\ &= \sum_{r=1}^n \int_{B^{(r)}} \nabla_{\mathbf{y}} \dot{\phi}^{(r)} \cdot \mathbf{p}^{(r)} \, dv \\ &\quad - \sum_{r=0}^{n-1} \sum_{s=r+1}^n \int_{\partial B^{(r)} \cap \partial B^{(s)}} \left[\mathbf{T}_M \hat{\mathbf{n}} \right] \cdot \mathbf{v} \, ds. \end{aligned}$$

Subtracting Eq. (2.40) from Eq. (2.35), we have

$$\begin{aligned} \frac{d}{dt} \left[\frac{1}{2} \sum_{r=0}^n \int_{B^{(r)}} \epsilon_0 |\mathbf{E}^{(r)}|^2 dv \right] &= - \sum_{r=1}^n \int_{B^{(r)}} \left(\nabla_{\mathbf{y}} \cdot \mathbf{T}_M^{(r)} \right) \cdot \mathbf{v} dv - \sum_{r=1}^n \int_{\Omega^{(r)}} \mathbf{E}^{(r)} \cdot \dot{\mathbf{p}}_0^{(r)} dV \\ &\quad + \hat{\phi} \frac{d}{dt} \int_{S_v} q ds + \sum_{r=0}^{n-1} \sum_{s=r+1}^n \int_{\partial B^{(r)} \cap \partial B^{(s)}} \llbracket \mathbf{T}_M \hat{\mathbf{n}} \rrbracket \cdot \mathbf{v} ds. \end{aligned} \quad (2.41)$$

2.3.5 Rate of dissipation: the final expression

Combining together Eqs. (2.25), (2.32) and (2.41) in (2.23), we arrive at

$$\begin{aligned} \mathcal{D} &= \mathcal{F} - \frac{d\mathcal{E}}{dt} \\ &= - \sum_{r=1}^n \int_{\Omega^{(r)}} \left[\frac{\partial W^{(r)}}{\partial \mathbf{p}_0} - \mathbf{E}^{(r)} \right] \cdot \dot{\mathbf{p}}_0^{(r)} dV \\ &\quad + \sum_{r=1}^n \int_{B^{(r)}} \left[\nabla_{\mathbf{y}} \cdot \mathbf{T}^{(r)} + \nabla_{\mathbf{y}} \cdot \mathbf{T}_M^{(r)} \right] \cdot \mathbf{v} dv \\ &\quad - \sum_{r=0}^{n-1} \sum_{s=r+1}^n \int_{\partial B^{(r)} \cap \partial B^{(s)}} \llbracket \mathbf{T} \hat{\mathbf{n}} + \mathbf{T}_M \hat{\mathbf{n}} \rrbracket \cdot \mathbf{v} ds + \sum_{r=1}^n \int_{\partial B^{(r)} \cap \partial B^{(0)}} \mathbf{t} \cdot \mathbf{v} ds. \end{aligned} \quad (2.42)$$

The boundary terms in Eq. (2.42) can be divided as follows

$$\begin{aligned} &- \sum_{r=0}^{n-1} \sum_{s=r+1}^n \int_{\partial B^{(r)} \cap \partial B^{(s)}} \llbracket \mathbf{T} \hat{\mathbf{n}} + \mathbf{T}_M \hat{\mathbf{n}} \rrbracket \cdot \mathbf{v} ds + \sum_{r=1}^n \int_{\partial B^{(r)} \cap \partial B^{(0)}} \mathbf{t} \cdot \mathbf{v} ds \\ &= - \sum_{r=1}^{n-1} \sum_{s=r+1}^n \int_{\partial B^{(r)} \cap \partial B^{(s)}} \llbracket \mathbf{T} \hat{\mathbf{n}} + \mathbf{T}_M \hat{\mathbf{n}} \rrbracket \cdot \mathbf{v} ds + \int_{\partial B} \left[\mathbf{t} - \left(\mathbf{T}^{(r)} + \mathbf{T}_M^{(r)} - \mathbf{T}_M^{(0)} \right) \hat{\mathbf{n}} \right] \cdot \mathbf{v} ds. \end{aligned} \quad (2.43)$$

The final expression for the rate of dissipation of the whole system is

$$\begin{aligned} \mathcal{D} &= - \sum_{r=1}^n \int_{\Omega^{(r)}} \left[\frac{\partial W^{(r)}}{\partial \mathbf{p}_0} - \mathbf{E}^{(r)} \right] \cdot \dot{\mathbf{p}}_0^{(r)} dV \\ &\quad + \sum_{r=1}^n \int_{B^{(r)}} \left[\nabla_{\mathbf{y}} \cdot \mathbf{T}^{(r)} + \nabla_{\mathbf{y}} \cdot \mathbf{T}_M^{(r)} \right] \cdot \mathbf{v} dv \\ &\quad - \sum_{r=1}^{n-1} \sum_{s=r+1}^n \int_{\partial B^{(r)} \cap \partial B^{(s)}} \llbracket \mathbf{T} \hat{\mathbf{n}} + \mathbf{T}_M \hat{\mathbf{n}} \rrbracket \cdot \mathbf{v} ds + \int_{\partial B} \left[\mathbf{t} - \left(\mathbf{T}^{(r)} + \mathbf{T}_M^{(r)} - \mathbf{T}_M^{(0)} \right) \hat{\mathbf{n}} \right] \cdot \mathbf{v} ds. \end{aligned} \quad (2.44)$$

From Eq. (2.44), we can see that the dissipation of the system has two contributions: the first integral is the dissipation caused by the polarization evolution, and

the remaining terms are the contribution from the deformation of the heterogeneous body. For convenience we define

$$\boldsymbol{\sigma}^{(r)} = \mathbf{T}^{(r)} + \mathbf{T}_M^{(r)} \quad (2.45)$$

to denote the *total stress tensor* which is the sum of the Cauchy and Maxwell stress tensors.

2.4 Governing equations

According to the variational principle “If $\int [g(x)h(x)]dx = 0 \quad \forall h(x)$, where $g(x)$ and $h(x)$ are continuous functions, then $g(x) = 0$ ”. In Eq. (2.44), we note that $\dot{\mathbf{p}}_0^{(r)}$ and \mathbf{v} are independent variables. Consequently, regarding the second law of thermodynamic, we conclude that the differential form of the governing equations can be expressed in the form

$$\frac{\partial W^{(r)}}{\partial \mathbf{p}_0} - \mathbf{E}^{(r)} = \mathbf{0} \quad \text{in } \Omega^{(r)}, \quad (2.46)$$

$$\nabla_{\mathbf{y}} \cdot \left(\mathbf{T}^{(r)} + \mathbf{T}_M^{(r)} \right) = \mathbf{0} \quad \text{in } B^{(r)}. \quad (2.47)$$

These two equations need to be solved together with Maxwell equation (2.1) and the corresponding boundary conditions. The additional boundary conditions extracted from Eq. (2.44) are

$$\left(\mathbf{T}^{(r)} + \mathbf{T}_M^{(r)} - \mathbf{T}_M^{(0)} \right) \hat{\mathbf{n}} = \mathbf{t} \quad \text{on } \partial B \cap \partial B^{(r)}, \quad (2.48)$$

and

$$\left(\mathbf{T}^{(s)} - \mathbf{T}^{(r)} \right) \hat{\mathbf{n}} = - \left(\mathbf{T}_M^{(s)} - \mathbf{T}_M^{(r)} \right) \hat{\mathbf{n}} \quad \text{on } \partial B^{(r)} \cap \partial B^{(s)}. \quad (2.49)$$

We note in Eqs. (2.47) and (2.49) that the total stress tensor $\boldsymbol{\sigma}$ is self-equilibrated in $B^{(r)}$ and continuous across the interfaces between the phases. Explicitly

$$\nabla_{\mathbf{y}} \cdot \boldsymbol{\sigma}^{(r)} = \mathbf{0} \quad \text{in } B^{(r)}, \quad (2.50)$$

and

$$\boldsymbol{\sigma}^{(s)} \hat{\mathbf{n}} = \boldsymbol{\sigma}^{(r)} \hat{\mathbf{n}} \quad \text{on } \partial B^{(r)} \cap \partial B^{(s)}. \quad (2.51)$$

3. APPLICATIONS TO EAPCS

The general variational principle of Chapter [2] is applied in this Chapter to determine the actuation strains of typical electroactive actuators made out of a layer of heterogeneous dielectric solid between two flat and thin electrodes (*e.g.*, Fig. 2.2).

To this end we make the following assumptions:

1. The characteristic size of the heterogeneity is much smaller than the size of the actuator.
2. The morphology of the actuator is such that the heterogeneous dielectric is macroscopically homogeneous.
3. The two electrodes remain straight and parallel during the deformation of the actuator.
4. The electrodes are flexible with a negligible elastic moduli and thus do not extract mechanical traction on the dielectric layer (*e.g.*, Bhattacharya et al., 2001).
5. We consider the deformation of the actuator due to electromechanical coupling but with no external loads. Accordingly, the traction boundary condition is $\mathbf{t} = \mathbf{0}$.
6. The size of the circumferential boundaries of the layer is considerably smaller than the size of the top and bottom boundaries which are in contact with the electrodes. Thus, we neglect edge or fringing effects due to the potential field induced by the electrodes in $B^{(0)}$, and assume that the electric field outside $\mathbf{y}(B)$ vanishes identically.
7. Only the coupling due to the Maxwell stress is accounted for.

We note that with the above assumptions the boundary conditions applied to the actuator are such that if it was made out of a homogeneous material the electrical fields within the actuator were uniform. These type of boundary conditions are commonly being used to determine the effective properties of composite materials. It can be shown that if the potential difference between the two electrodes is $\hat{\phi} = -\mathbf{E}_0 \cdot \mathbf{y}$, then the mean electric field

$$\bar{\mathbf{E}} \equiv \frac{1}{v} \sum_{r=1}^n \int_{B^{(r)}} \mathbf{E}^{(r)} dv = \mathbf{E}_0, \quad (3.1)$$

where v is the volume of the composite in the deformed configuration. Since we assumed that the composite is macroscopically homogeneous, to determine the electric fields developing in the composite it is sufficient to consider a unit volume element (in the deformed configuration) which is representative of the composite microstructure and yet considerably smaller than the overall size of the actuator. We require that within the unit volume element $\bar{\mathbf{E}} = \mathbf{E}_0$, and thus ensure that the far field boundary condition is satisfied in an average sense. With this requirement we need to solve Maxwell equation (2.1) in the unit element together with the continuity conditions (2.10) and (2.9) and the constitutive relation (2.46) for a given realization $\mathbf{y}(B)$ in \mathbb{R}^3 .

Once the electric and electric displacement fields are determined, the corresponding Maxwell stresses developing in the phases can be determined too. In the actuator we consider, this is precisely the electrical excitation which results in the actuation of the EAPC. We note that due to the contrast in the properties of the phases there are local fluctuations in the intensity of the Maxwell stress. However, since the actuator is macroscopically homogeneous, at a scale which is much larger than the characteristic size of the phases, the overall effect of Maxwell stress can be viewed as macroscopically homogeneous. In particular, this reinforces assumption (3) above that the two electrodes will remain parallel during the deformation caused by the electrical excitation. Together with assumption (5) above concerning the traction boundary conditions, it follows that the macroscopic deformation gradient \mathbf{A}_0 is a constant matrix with $\det(\mathbf{A}_0) \equiv J_0 > 0$.

Following Hill (1972), Hill and Rice (1973), and Ogden (1974) who considered the problem of heterogeneous elastic solids undergoing large deformations, in a reference unit volume of a representative element $\Omega_0 \subset \Omega$,

$$\bar{\mathbf{A}} \equiv \sum_{r=1}^n \int_{\Omega_0^{(r)}} \mathbf{A}^{(r)} dV = \mathbf{A}_0, \quad (3.2)$$

where $\Omega_0^{(r)} = \Omega_0 \cap \Omega^{(r)}$. Clearly $J_0 = \bar{J}$. From Eq. (2.30) we note that the stress measure conjugate to the deformation gradient is the nominal stress (or the first Piola-Kirchhoff stress), and hence averages of the stress must be determined in the reference configuration (*e.g.*, Hill, 1972). Accordingly, the Maxwell stresses, which are determined in the deformed configuration, must be “pulled back” in each phase and added to the nominal mechanical stresses in the reference configuration. We carry out the above calculations by using Nanson’s formula together with Eq. (2.48) and require that in a reference unit volume of a representative element,

$$\bar{\mathbf{T}} \equiv \bar{\mathbf{\Sigma}} + \sum_{r=1}^n \int_{\Omega_0^{(r)}} J^{(r)} \mathbf{T}_M^{(r)} (\mathbf{A}^{(r)})^{-T} dV = \mathbf{0}. \quad (3.3)$$

Here

$$\bar{\mathbf{\Sigma}} \equiv \sum_{r=1}^n \int_{\Omega_0^{(r)}} \mathbf{\Sigma}^{(r)} dV, \quad (3.4)$$

is the average nominal stress and

$$\mathbf{\Sigma}^{(r)} = J^{(r)} \mathbf{T}^{(r)} (\mathbf{A}^{(r)})^{-T} \quad (3.5)$$

are the nominal stresses in the phases. Eq. (3.3) results from the boundary condition Eq. (2.48) specialized to the case $\mathbf{t} = \mathbf{0}$ and $\mathbf{T}_M^{(0)} = \mathbf{0}$ in accordance with assumptions (5) and (6).

To determine the macroscopic actuation $\mathbf{A}_0 = \bar{\mathbf{A}}$, we need to solve the governing equilibrium equation (2.47) together with the continuity conditions (2.49), the boundary condition Eq. (3.3) and the average equation (3.2). This set of equations should be solved for the unknowns $\mathbf{A}^{(r)}$.

For later use we recall that the volume fraction of the r -phase in the composite is

$$\lambda^{(r)} = \frac{1}{V} \int_{\Omega} \chi^{(r)}(\mathbf{x}) dV. \quad (3.6)$$

3.1 Heterogeneous hyperelastic dielectric

In this work we consider the class of composites made out of incompressible neo-Hookean phases with strain energy-density functions

$$W_0^{(r)}(\mathbf{A}, \mathbf{p}_0) = \frac{1}{2}\mu^{(r)}\text{Tr}(\mathbf{A}\mathbf{A}^T - \mathbf{I}) + \left(\frac{1}{8\pi\epsilon_0}(\boldsymbol{\chi}^{(r)})^{-1}\mathbf{p}_0\right) \cdot \mathbf{p}_0. \quad (3.7)$$

Here $\mu^{(r)}$ is the shear modulus and $\boldsymbol{\chi}^{(r)}$ is the electric *susceptibility* matrix of the r -phase. The symmetric susceptibility tensor is related to the *dielectric* tensor, or relative *permittivity* tensor, \mathbf{k} by

$$\mathbf{k} = \mathbf{I} + 4\pi\boldsymbol{\chi}. \quad (3.8)$$

Since the phases are incompressible, it follows from Eq. (2.3) that $\mathbf{p}(\mathbf{y}(\mathbf{x})) = \mathbf{p}_0(\mathbf{x})$ and hence, from Eq. (2.46), that at a material point $\mathbf{y}(\mathbf{x}) \in B^{(r)}$, the electric field is

$$\mathbf{E}^{(r)} = \frac{1}{4\pi\epsilon_0}(\boldsymbol{\chi}^{(r)})^{-1}\mathbf{p}^{(r)}. \quad (3.9)$$

Hence by using Eqs. (2.2), (3.8) and (3.9) the electric displacement field is

$$\mathbf{D}^{(r)} = \epsilon_0\mathbf{k}^{(r)}\mathbf{E}^{(r)}. \quad (3.10)$$

Putting together Eqs. (2.17) and (3.10) we can determine the Maxwell stress in the form

$$\mathbf{T}_M^{(r)} = \mathbf{B}^{(r)} : \mathbf{E}^{(r)} \otimes \mathbf{E}^{(r)}, \quad (3.11)$$

where

$$B_{ijkl}^{(r)} = \epsilon_0 k_{jl}^{(r)}\delta_{ki} - \frac{\epsilon_0}{2}\delta_{ij}\delta_{kl}, \quad (3.12)$$

and δ_{ij} is the Kronecker delta. In index notation the double contraction of a fourth-order tensor \mathbf{M} with a second-order tensor \mathbf{N} , is $(\mathbf{M} : \mathbf{N})_{ij} = M_{ijkl}N_{kl}$.

The corresponding mechanical constitutive law for the nominal stress in terms of the deformation gradient is

$$\boldsymbol{\Sigma}^{(r)} = \mu^{(r)}\mathbf{A} - p^{(r)}\mathbf{A}^{-T}, \quad (3.13)$$

where $p^{(r)}$ is an arbitrary hydrostatic pressure, and the expression for the Cauchy stress tensor is

$$\mathbf{T}^{(r)} = \mu^{(r)}\mathbf{A}\mathbf{A}^T - p^{(r)}\mathbf{I}. \quad (3.14)$$

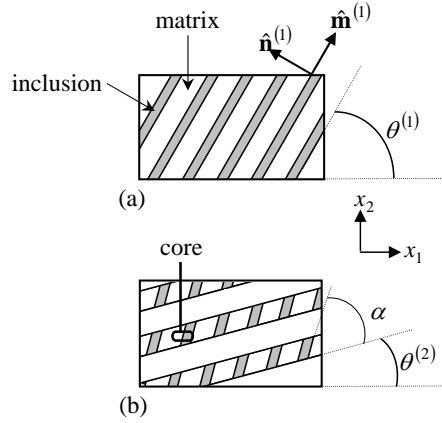


Fig. 3.1: (a) A rank-1 and (b) a rank-2 laminated composites.

Using these constitutive relations and the above formulation we can determine the response of incompressible neo-Hookean dielectric composites. In the following Subsection we present the solution for a simple case such as laminated composites. In this idealized microstructure, explicit expression for the electromechanical response can be obtained.

3.1.1 Solution for hyperelastic laminated EAPCs

A simple laminated composite, denoted as rank-1 laminate, is constructed by layering two materials in an alternate order (see Fig. 3.1a). A rank-2 laminate is constructed by layering a rank-1 composite as a core phase with another constituent phase, or with one of the original phases, as illustrated in Fig. 3.1b. A rank- N composite is constructed by following this procedure N times.

Consider a rank-1 laminate made out of two phases with energy-density functions like in Eq. (3.7), in volume fractions $\lambda^{(i)}$ and $\lambda^{(m)} = 1 - \lambda^{(i)}$, respectively. The direction normal to the layers plane (in the deformed configuration) is defined as the laminate direction ($\hat{\mathbf{n}}^{(1)}$ in Fig. 3.1). We assume that the actuator is subjected to plane strain loading conditions such that for any $\mathbf{y} \in B$, $y_i(\mathbf{x}) = y_i(x_1, x_2)$ ($i = 1, 2$) and $y_3(\mathbf{x}) = x_3$.

First we consider the electrostatic problem. The mean electric field in the

laminate is

$$\bar{\mathbf{E}} = (1 - \lambda^{(i)}) \mathbf{E}^{(m)} + \lambda^{(i)} \mathbf{E}^{(i)}, \quad (3.15)$$

where we recall that $\mathbf{E}^{(m)}$ and $\mathbf{E}^{(i)}$ are uniform within each phase. From the continuity condition (2.8) it follows that

$$(\mathbf{E}^{(m)} - \mathbf{E}^{(i)}) \cdot \hat{\mathbf{m}}^{(1)} = 0, \quad (3.16)$$

where $\hat{\mathbf{m}}^{(1)}$ is a unit vector (in the deformed configuration) tangent to the interface. Thus, we can write the electric field in each phase in the form

$$\begin{aligned} \mathbf{E}^{(m)} &= \bar{\mathbf{E}} + \beta^{(1)} \lambda^{(i)} \hat{\mathbf{n}}^{(1)}, \\ \mathbf{E}^{(i)} &= \bar{\mathbf{E}} - \beta^{(1)} (1 - \lambda^{(i)}) \hat{\mathbf{n}}^{(1)}, \end{aligned} \quad (3.17)$$

where β is a scalar and the superscript (1) identifies quantities associated with the rank-1 composite. When the interface is charge free, from the continuity condition (2.10)

$$(\mathbf{D}^{(m)} - \mathbf{D}^{(i)}) \cdot \hat{\mathbf{n}}^{(1)} = 0. \quad (3.18)$$

Upon substitution of the linear constitutive relation (3.10) and expressions (3.17) in Eq. (3.18), we obtain the following expression for $\beta^{(1)}$

$$\beta^{(1)} = - \frac{(\mathbf{k}^{(m)} - \mathbf{k}^{(i)}) : (\hat{\mathbf{n}}^{(1)} \otimes \bar{\mathbf{E}})}{[\lambda^{(i)} \mathbf{k}^{(m)} + (1 - \lambda^{(i)}) \mathbf{k}^{(i)}] : (\hat{\mathbf{n}}^{(1)} \otimes \hat{\mathbf{n}}^{(1)})}. \quad (3.19)$$

Analogous procedure is followed for the mechanical problem but quantities are represented in the reference configuration. Thus, since the displacement fields in the phases are uniform, the macroscopic deformation gradient tensor is

$$\bar{\mathbf{A}} = (1 - \lambda^{(i)}) \mathbf{A}^{(m)} + \lambda^{(i)} \mathbf{A}^{(i)}. \quad (3.20)$$

The deformation continuity condition implies that along the interface

$$(\mathbf{A}^{(m)} - \mathbf{A}^{(i)}) \hat{\mathbf{M}}^{(1)} = \mathbf{0}, \quad (3.21)$$

where $\hat{\mathbf{M}}^{(1)}$ is a unit vector in the layers plane in the reference configuration. Following deBotton (2005), due to the incompressibility assumption and the plane

strain loading state, the deformation gradients in the phases of the laminate can be expressed in the form

$$\begin{aligned}\mathbf{A}^{(m)} &= \bar{\mathbf{A}} \left(\mathbf{I} + \omega^{(1)} \lambda^{(i)} \hat{\mathbf{M}}^{(1)} \otimes \hat{\mathbf{N}}^{(1)} \right), \\ \mathbf{A}^{(i)} &= \bar{\mathbf{A}} \left(\mathbf{I} - \omega^{(1)} (1 - \lambda^{(i)}) \hat{\mathbf{M}}^{(1)} \otimes \hat{\mathbf{N}}^{(1)} \right),\end{aligned}\quad (3.22)$$

where $\omega^{(1)}$ is a scalar and $\hat{\mathbf{N}}^{(1)}$ is the unit vector normal to the layers-plane in the reference configuration. From Eq. (2.49) it follows that the traction continuity condition in the reference configuration is

$$(\boldsymbol{\Sigma}^{(m)} - \boldsymbol{\Sigma}^{(i)}) \hat{\mathbf{N}}^{(1)} = - \left[\mathbf{T}_M^{(m)} (\mathbf{A}^{(m)})^{-T} - \mathbf{T}_M^{(i)} (\mathbf{A}^{(i)})^{-T} \right] \hat{\mathbf{N}}^{(1)}. \quad (3.23)$$

Putting together Eqs. (3.11), (3.13), (3.17) and (3.22) and the relation $\hat{\mathbf{n}}^{(1)} = \bar{\mathbf{A}}^{-T} \hat{\mathbf{N}}^{(1)}$ in Eq. (3.23) we obtain an equation for $\omega^{(1)}$ and $\Delta p = p^{(m)} - p^{(i)}$.

By taking the dot product of the above equation with $\bar{\mathbf{A}} \hat{\mathbf{M}}^{(1)}$, an explicit expression for $\omega^{(1)}$ is determined, namely,

$$\omega^{(1)} = - \frac{\mu^{(m)} - \mu^{(i)}}{\lambda^{(i)} \mu^{(m)} + (1 - \lambda^{(i)}) \mu^{(i)}} \frac{\bar{\mathbf{A}} \hat{\mathbf{N}}^{(1)} \cdot \bar{\mathbf{A}} \hat{\mathbf{M}}^{(1)}}{\bar{\mathbf{A}} \hat{\mathbf{M}}^{(1)} \cdot \bar{\mathbf{A}} \hat{\mathbf{M}}^{(1)}}. \quad (3.24)$$

A similar procedure can be repeated to derive an explicit expression for Δp . This done by taking the dot product of Eq. (3.23) with $\bar{\mathbf{A}}^{-T} \hat{\mathbf{N}}^{(1)}$.

Now we can write the expression for the total nominal macroscopic stress in terms of the overall deformation gradient $\bar{\mathbf{A}}$ and the applied electric field $\bar{\mathbf{E}}$ in the form

$$\begin{aligned}\bar{\boldsymbol{\Gamma}} &= \\ & (1 - \lambda^{(i)}) \left[\mu^{(m)} \bar{\mathbf{A}} \left(\mathbf{I} + \omega^{(1)} \lambda^{(i)} \hat{\mathbf{M}}^{(1)} \otimes \hat{\mathbf{N}}^{(1)} \right) \right] + \\ & \lambda^{(i)} \left[\mu^{(i)} \bar{\mathbf{A}} \left(\mathbf{I} - \omega^{(1)} (1 - \lambda^{(i)}) \hat{\mathbf{M}}^{(1)} \otimes \hat{\mathbf{N}}^{(1)} \right) \right] + \\ & (1 - \lambda^{(i)}) \left(\mathbf{T}_M^{(m)} - (\bar{p} + \lambda^{(i)} \Delta p) \right) \bar{\mathbf{A}}^{-T} (\mathbf{I} - \omega^{(1)} \lambda^{(i)} \hat{\mathbf{N}}^{(1)} \otimes \hat{\mathbf{M}}^{(1)}) + \\ & \lambda^{(i)} \left(\mathbf{T}_M^{(i)} - (\bar{p} - (1 - \lambda^{(i)}) \Delta p) \right) \bar{\mathbf{A}}^{-T} (\mathbf{I} + \omega^{(1)} (1 - \lambda^{(i)}) \hat{\mathbf{N}}^{(1)} \otimes \hat{\mathbf{M}}^{(1)}),\end{aligned}\quad (3.25)$$

where the expressions for the Maxwell stresses in the two phases are

$$\begin{aligned}\mathbf{T}_M^{(m)} &= \mathbf{B}^{(m)} : \left[\left(\bar{\mathbf{E}} + \beta^{(1)} \lambda^{(i)} \bar{\mathbf{A}}^{-T} \hat{\mathbf{N}}^{(1)} \right) \otimes \left(\bar{\mathbf{E}} + \beta^{(1)} \lambda^{(i)} \bar{\mathbf{A}}^{-T} \hat{\mathbf{N}}^{(1)} \right) \right] \\ \mathbf{T}_M^{(i)} &= \mathbf{B}^{(i)} : \left[\left(\bar{\mathbf{E}} - \beta^{(1)} (1 - \lambda^{(i)}) \bar{\mathbf{A}}^{-T} \hat{\mathbf{N}}^{(1)} \right) \otimes \left(\bar{\mathbf{E}} - \beta^{(1)} (1 - \lambda^{(i)}) \bar{\mathbf{A}}^{-T} \hat{\mathbf{N}}^{(1)} \right) \right].\end{aligned}\quad (3.26)$$

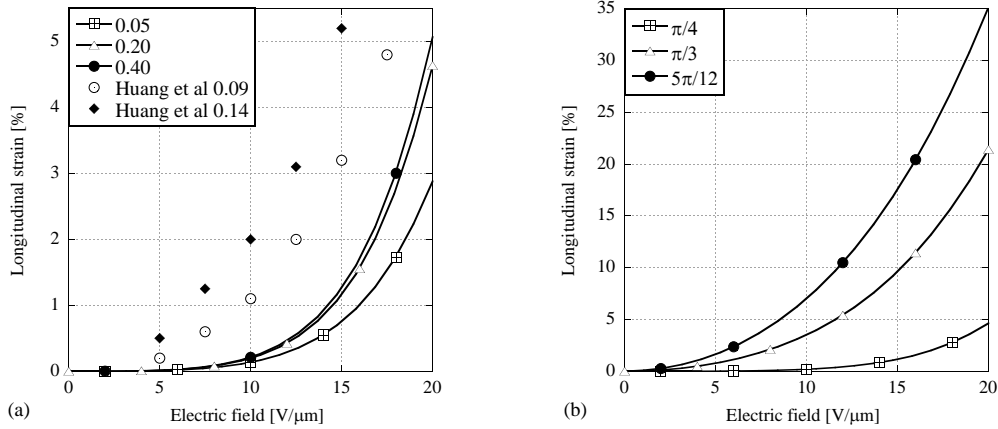


Fig. 3.2: Experimental measurements of Huang et al. (2004) and analytical predictions of the actuation strain of EAPCs as a function of the electric excitation field. Figures (a) and (b) demonstrate the variations due to changes in the volume fraction of the inclusions phase and the lamination angle, respectively.

Here, \bar{p} is the (indeterminate) macroscopic pressure, and $\beta^{(1)}$ and $\omega^{(1)}$ are given in expressions (3.19) and (3.24), respectively.

3.1.2 Examples

By application of Eq. (3.25) to the case of traction free boundary conditions, we determine the response of an actuator made out of laminated EAPC (Fig. 3.1a). Due to the induced electric field, Maxwell stresses develop in the two phases and the actuator contracts along its thickness (x_2 axis) and expands along its longer dimension (x_1 axis). According to assumption (3) the top and bottom electrodes remain parallel ($\bar{A}_{21} = 0$), and we further assume that the intensity of the applied electric field ($\bar{E}_2 = E_0$) is known in the deformed configuration. For convenience, following common practice in the field of electroactive materials we examine the longitudinal “actuation” strains (the Eulerian strain \bar{E}_{11} in Fig. 2.2) developing in the composites due to the electrostatic field between the electrodes (*e.g.*, Bhat-tacharya et al., 2001; McMeeking and Landis, 2005).

Shown in Fig. 3.2 is the longitudinal strain response of rank-1 EAPCs with phases whose properties are similar to those in the composites investigated experimentally by Huang et al. (2004). This serves to demonstrate the ability to simulate

the behavior of the actuators. Here, the “*inclusions*” phase has properties resembling those of the PolyCuPc oligomer host particles (*i.e.*, $\mu^{(i)} = 660[\text{MPa}]$ and $k^{(i)} = 0.25 \cdot 10^6$) and the “*matrix*” phase has properties analogous to the flexible PU polymer with a shear modulus $\mu^{(m)} = 10[\text{MPa}]$ and a dielectric constant $k^{(m)} = 8$. Since the PolyCuPc particles are essentially conducting, this idealized rank-1 model is realistic only if the actuator is isolated (otherwise current will flow between the electrodes resulting in $\bar{E}_2 = 0$). In Fig. 3.2a the effect of increasing the volume fraction of the inclusions phase is demonstrated for EAPCs with lamination direction of $\pi/4$. We note the quadratic dependence of the strains on the applied electric field. For the 20% PolyCuPc actuator there is only a negligible response up to $\bar{E}_2 = 10[\text{V}/\mu\text{m}]$, from there on the response is accelerated up to 5% strain under activation field of $20[\text{V}/\mu\text{m}]$. The trend of these curves and the magnitude of the strains are in agreement with the corresponding experimental results (Fig. 3a of Huang et al., 2004). However, the magnitudes of the predicted strains are lower than those measured in the experiments. These differences can be attributed to the different morphologies of the measured and analyzed composites, and to the fact that electrostriction effects are not accounted for in the present analysis. Changes in the volume fraction of the PolyCuPc phase have relatively small effect on the overall response of the EAPC. More pronounced are the variations due to the changes in the lamination direction. In Fig. 3.2b the dependence of the EAPC with $\lambda^{(i)} = 0.2$ response on the morphology is demonstrated. As the lamination angle is increased the actuator becomes more responsive. This is not surprising in view of the fact that the effective dielectric constant of the actuator approaches the Voigt upper bound resulting in large electric displacement fields and hence in large stresses and strains.

We consider a second case which highlights the idea that with an appropriate design of the microstructure the EAPC can do *better than its constituents*. A rank-1 composite is made out of a stiff phase with high-dielectric constant and a soft phase with low-dielectric constant. The properties chosen are representative of values of real dielectrics and both phases have the same electrostatic strain response (the

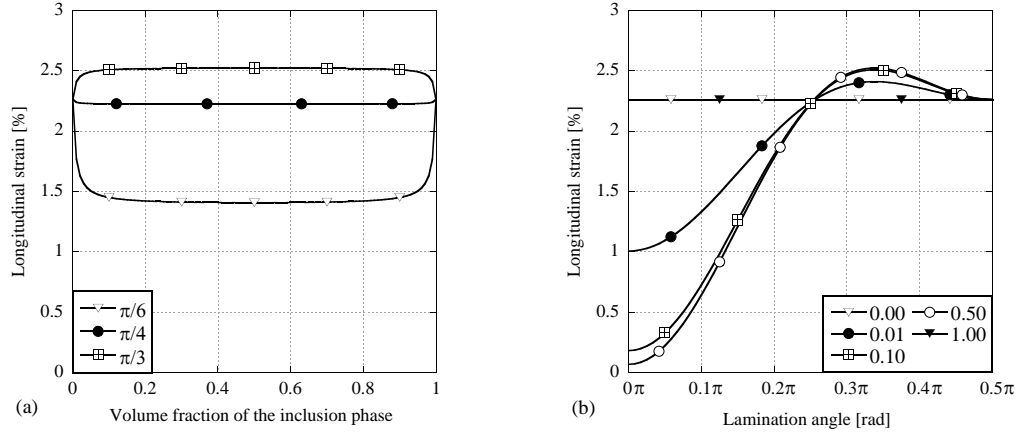


Fig. 3.3: Actuation strain of a laminated EAPC with stiff and compliant phases whose electrostatic strain responses are identical. Figure (a) demonstrates the variations as functions of the inclusions' volume fraction for fixed lamination angles, and (b) variations due to different lamination angles for a few fixed inclusions' volume fractions, respectively.

ratio of the shear to the dielectric moduli are the same *i.e.*, $k^{(i)}/\mu^{(i)} = k^{(m)}/\mu^{(m)}$). Specifically, the properties of the matrix phase are $\mu^{(m)} = 8[\text{MPa}]$ and $k^{(m)} = 8$, and the dielectric and shear moduli of the inclusions phase are $\mu^{(i)} = 1000[\text{MPa}]$ and $k^{(i)} = 1000$, respectively. Results, in terms of actuation strains as function of the volume fraction of the stiff phase, are shown in Fig. 3.3a for a fixed activation field $\bar{E}_2 = 100[\text{V}/\mu\text{m}]$. We note that the volume fraction of the phases have only small influence on the effective strain response. This is because the effective stiffness and the dielectric tensor of the EAPC are changing in the same fashion (as we assume that the electric field is fixed, the intensity of the Maxwell stresses is proportional to the dielectric constant). However, as further demonstrated in Fig. 3.3b, the lamination direction has a large impact on the overall response of the EAPC. For all volume fractions, at low lamination angles the response of the EAPC is lower than that of its phases (the horizontal line representing the response of a homogeneous EAP with volume fraction $\lambda^{(i)} = 0$ or $\lambda^{(i)} = 1$). On the other hand, when the lamination angle is larger than $\pi/4$ an *amplification* of the actuation strain is obtained. In particular, with $\lambda^{(i)} = 0.1$ and lamination angle $\pi/3$ the EAPC actuation strain is 10% higher than the actuation strain of its constituting phases.

It is anticipated that the number of actual EAPCs microstructures and constituents behaviors for which analytical solutions can be determined, in the form described in Section 3.1.1, is fairly small. Socolsky (2007) obtained an explicit expression for the macroscopic electromechanical response of hyperelastic dielectric rank-2 composites (*e.g.*, Fig. 3.1b). This procedure can be repeated to determine the behavior of sequentially laminated composites undergoing large deformations. In this work we will consider this class of composites but in the limit of small deformation elasticity. Another approach to treat this highly nonlinear problem is by providing a numerical tool. This will be done in Chapter 4.

3.2 The limit of small deformations elasticity

As was demonstrate in the previous Section there are only a few cases of EAPCs which can be solved analytically. However in the limit of small deformations the situation is simpler. Thus, as a step towards a better understanding of the role of the microstructure in the nonlinear coupling phenomenon, it is helpful to analyze the response of heterogeneous materials in the limit of infinitesimal elasticity (*e.g.*, Li and Rao, 2004; Nan and Weng, 2000, for the electrostriction coupling effect). To further reveal the parameters at the microscopic level which influence the macroscopic behavior of the EAPC, in the following Section we generalize the works of Levin (1967) and Rosen and Hashin (1970) for determining the effective thermoelastic responses of two-phase and multiphase composites, respectively. To this end we follow the formulation of Chapter 2 but in the limit of small deformation elasticity.

We assume that the deformation within the homogeneous phases is characterized in terms of the (infinitesimal) strain tensor

$$\boldsymbol{\varepsilon}^{(r)} = \frac{1}{2} \left[\nabla \mathbf{u} + (\nabla \mathbf{u})^T \right], \quad (3.27)$$

where the displacement vector \mathbf{u} is continuous throughout the composite. Similar to Section 3.1, we consider composite dielectrics in which within the homogeneous phases the energy-density functions $W^{(r)}$ depend on the polarization vector and

the strain tensor

$$W^{(r)}(\mathbf{p}, \boldsymbol{\varepsilon}) = \frac{1}{2} \boldsymbol{\varepsilon} : \mathbf{L}^{(r)} : \boldsymbol{\varepsilon} + \left(\frac{1}{8\pi\epsilon_0} (\boldsymbol{\chi}^{(r)})^{-1} \mathbf{p} \right) \cdot \mathbf{p}, \quad (3.28)$$

where $\mathbf{L}^{(r)}$ is the elastic tensor of the r -phase. The stress-strain relations within the phases resulting from Eq. (3.28) are

$$\mathbf{T}^{(r)} = \frac{\partial W^{(r)}}{\partial \boldsymbol{\varepsilon}} = \mathbf{L}^{(r)} : \boldsymbol{\varepsilon} \quad (3.29)$$

and the corresponding relations between the electric field and the polarization are identical to Eq. (3.9). This lends itself to the following coupled constitutive relation for the total stress in the homogeneous phases, namely

$$\boldsymbol{\sigma}^{(r)} = \mathbf{L}^{(r)} : \boldsymbol{\varepsilon} + \mathbf{B}^{(r)} : \mathbf{E} \otimes \mathbf{E}. \quad (3.30)$$

We recall that in numerous works definitions of the overall relations between the applied electric field $\bar{\mathbf{E}}$ and the resulting mean electric displacement $\bar{\mathbf{D}}$ are given in terms of an effective dielectric tensor $\tilde{\mathbf{k}}$. Exact relations, estimates and bounds on $\tilde{\mathbf{k}}$ for many classes of composites with various microstructures are available too. Analogous results for the corresponding mechanical problem, where the averages of the stress $\bar{\mathbf{T}}$ and the strain $\bar{\boldsymbol{\varepsilon}}$ fields in a composite are related through an effective elasticity tensor $\tilde{\mathbf{L}}$, can be found in the literature too. Many of the pertinent results are summarized in the monograph by Milton (2002) and references therein. In this Section our first goal is to define the macroscopic coupled electromechanical response of the composite.

We begin by considering a homogeneous dielectric subjected to *electrostatic* loading. Thus, it is subjected to the boundary conditions $\mathbf{u}^0(\mathbf{x}) = \mathbf{0}$ and $\phi(\mathbf{x}) = -\mathbf{E}^0 \cdot \mathbf{x}$ on its boundary. The resulting strain in the body is $\boldsymbol{\varepsilon}^0 = \mathbf{0}$ and the uniform electric field is $\mathbf{E}(\mathbf{x}) = \mathbf{E}^0$. The total stress in the body is uniform and it follows from Eq. (3.30) that under this type of loading the uniform stress in the body is equal to the Maxwell stress, that is

$$\boldsymbol{\sigma}^0 = \mathbf{B} : \mathbf{E}^0 \otimes \mathbf{E}^0 \equiv \mathbf{T}_M^0. \quad (3.31)$$

Consider next a composite made out of n phases with quadratic stored energy-density functions as in Eq. (3.28). The composite is subjected to two types of

boundary conditions. The first is an electrostatic loading as before (*i.e.*, $\phi(\partial\Omega) = -\bar{\mathbf{E}}^0 \cdot \mathbf{x}$ and $\mathbf{u}^0(\partial\Omega) = \mathbf{0}$). The second boundary condition corresponds to *mechanical* loading with $\mathbf{u}'(\partial\Omega) = \bar{\boldsymbol{\varepsilon}}' \mathbf{x}$, where $\bar{\boldsymbol{\varepsilon}}'$ is a constant symmetric tensor, and $\phi'(\partial\Omega) = 0$. To avoid cumbersome notation we use the superscript “0” to identify macroscopic quantities that are related to the entire composite in the electrostatic problem. The corresponding quantities in the phases are not marked. The quantities associated with the mechanical boundary conditions are identified with a prime. Accordingly,

$$\int_{\Omega} \boldsymbol{\varepsilon}^0 : \boldsymbol{\sigma}' dV = \sum_{r=1}^n \int_{\Omega^{(r)}} \boldsymbol{\varepsilon}^{(r)} : \boldsymbol{\sigma}'^{(r)} dV. \quad (3.32)$$

With the aid of the divergence theorem (within the homogeneous phases) we split the right hand side of Eq. (3.32) into two parts

$$\int_{\Omega} \boldsymbol{\varepsilon}^0 : \boldsymbol{\sigma}' dV = \sum_{r=1}^n \int_{\partial\Omega^{(r)}} (\boldsymbol{\sigma}'^{(r)} \hat{\mathbf{n}}) \cdot \mathbf{u}^{(r)} ds - \sum_{r=1}^n \int_{\Omega^{(r)}} (\nabla \cdot \boldsymbol{\sigma}'^{(r)}) \cdot \mathbf{u}^{(r)} dV = 0. \quad (3.33)$$

We note that in $\Omega^{(r)}$, $\nabla \cdot \boldsymbol{\sigma}'^{(r)} = \mathbf{0}$, and on the composite’s boundary $\mathbf{u}^{(r)}(\partial\Omega) = \mathbf{u}^0(\partial\Omega) = \mathbf{0}$. From the continuity condition on the traction at the interfaces it follows that

$$\boldsymbol{\sigma}'^{(s)} \hat{\mathbf{n}}^{(s)} = -\boldsymbol{\sigma}'^{(r)} \hat{\mathbf{n}}^{(r)},$$

and since $\mathbf{u}^{(s)}(\mathbf{x}) = \mathbf{u}^{(r)}(\mathbf{x})$ on the interfaces, the sum of the terms in the right hand side of Eq. (3.33) vanishes.

In each phase $\boldsymbol{\sigma}^{(r)} = \mathbf{L}^{(r)} : \boldsymbol{\varepsilon}^{(r)} + \mathbf{T}_M^{(r)}$ for the electrostatic problem, and $\boldsymbol{\sigma}'^{(r)} = \mathbf{L}^{(r)} : \boldsymbol{\varepsilon}'^{(r)}$ under the purely mechanical boundary condition. Therefore, exploiting the linear stress strain relations in the purely mechanical problem, we have that

$$\int_{\Omega^{(r)}} \boldsymbol{\varepsilon}^{(r)} : \boldsymbol{\sigma}'^{(r)} dV = \int_{\Omega^{(r)}} \left(\boldsymbol{\sigma}^{(r)} - \mathbf{T}_M^{(r)} \right) : \boldsymbol{\varepsilon}'^{(r)} dV. \quad (3.34)$$

Hence, using Eqs. (3.32)-(3.34),

$$\int_{\Omega} \boldsymbol{\sigma}^0 : \boldsymbol{\varepsilon}' dV = \sum_{r=1}^n \int_{\Omega^{(r)}} \mathbf{T}_M^{(r)} : \boldsymbol{\varepsilon}'^{(r)} dV, \quad (3.35)$$

where $\boldsymbol{\varepsilon}'^{(r)}(\mathbf{x})$, $r = 1, 2, \dots, n$ are the well defined strains that develop in the phases under the purely mechanical boundary condition. Upon reusing the divergence

theorem in each phase and the fact that the traction $\boldsymbol{\sigma}^0 \hat{\mathbf{n}}$ is continuous across the interfaces, we have that

$$\begin{aligned} \int_{\Omega} \boldsymbol{\sigma}^0 : \boldsymbol{\varepsilon}' dV &= \int_{\partial\Omega} (\boldsymbol{\sigma}^0 \hat{\mathbf{n}}) \cdot \mathbf{u}' ds - \int_{\Omega} (\nabla \cdot \boldsymbol{\sigma}^0) \cdot \mathbf{u}' dV \\ &= \bar{\boldsymbol{\varepsilon}}' : \int_{\partial\Omega} (\boldsymbol{\sigma}^0 \hat{\mathbf{n}}) \cdot \mathbf{x} ds \\ &= \bar{\boldsymbol{\sigma}}^0 : \bar{\boldsymbol{\varepsilon}}'. \end{aligned} \quad (3.36)$$

Since the stress in the electrostatic boundary condition problem develops due to the electromechanical coupling (*e.g.*, Eq. (3.31) for the homogeneous body) it follows that the effective Maxwell stress in the composite can be defined via the relation

$$\bar{\mathbf{T}}_M^0 : \bar{\boldsymbol{\varepsilon}}' \equiv \bar{\boldsymbol{\sigma}}^0 : \bar{\boldsymbol{\varepsilon}}'. \quad (3.37)$$

Putting together Eqs. (3.35) and (3.37) we conclude that

$$\bar{\mathbf{T}}_M^0 : \bar{\boldsymbol{\varepsilon}}' = \sum_{r=1}^n \int_{\Omega^{(r)}} \mathbf{T}_M^{(r)} : \boldsymbol{\varepsilon}'^{(r)} dV. \quad (3.38)$$

In principle Eq. (3.38) together with expression (3.11) provides a systematic method for determining the macroscopic Maxwell stress $\bar{\mathbf{T}}_M^0$.

Moreover, in each phase the electric and the strain fields can be represented as the sum of their averages and the fluctuations about the average,

$$\begin{aligned} \mathbf{E}^{(r)} &= \bar{\mathbf{E}}^{(r)} + \Delta \mathbf{E}^{(r)} \\ \boldsymbol{\varepsilon}^{(r)} &= \bar{\boldsymbol{\varepsilon}}^{(r)} + \Delta \boldsymbol{\varepsilon}^{(r)}, \end{aligned} \quad (3.39)$$

where $\int_{\Omega^{(r)}} \Delta \mathbf{E}^{(r)} dV = 0$ and $\int_{\Omega^{(r)}} \Delta \boldsymbol{\varepsilon}^{(r)} dV = 0$. Thus, substituting Eq. (3.11) and (3.39) in (3.38), in each phase we find

$$\begin{aligned} \int_{\Omega^{(r)}} \mathbf{T}_M^{(r)} : \boldsymbol{\varepsilon}'^{(r)} dV &= \int_{\Omega^{(r)}} (\mathbf{B}^{(r)} : \mathbf{E}^{(r)} \otimes \mathbf{E}^{(r)}) : \boldsymbol{\varepsilon}'^{(r)} dV \\ &= V^{(r)} (\mathbf{B}^{(r)} : \bar{\mathbf{E}}^{(r)} \otimes \bar{\mathbf{E}}^{(r)}) : \bar{\boldsymbol{\varepsilon}}'^{(r)} \\ &\quad + \mathbf{B}^{(r)} : \left(\int_{\Omega^{(r)}} (2\bar{\mathbf{E}}^{(r)} \otimes \Delta \mathbf{E}^{(r)} : \Delta \boldsymbol{\varepsilon}'^{(r)} + \Delta \mathbf{E}^{(r)} \otimes \Delta \mathbf{E}^{(r)} : \boldsymbol{\varepsilon}'^{(r)}) dV \right). \end{aligned} \quad (3.40)$$

Naturally, the main difficulty is to determine the second term in expression (3.40), the term involving the fluctuations in the electric field. Li et al. (2004) found

that the field fluctuations in the matrix of an all-polymer percolative composite may lead to enhancement of the electromechanical coupling. In the composite they analyzed the large contrast between the dielectric constants of the two constituents resulted in large fluctuations of the electric field in the matrix, and hence to the amplification of the electromechanical coupling. We emphasize, however, that in the composite considered by Li et al. (2004) the matrix phase was *electrostrictive*, and the overall electromechanical coupling of the composite was mainly due to this property of the matrix phase. Contrariwise, if the coupling is due to the Maxwell stress, the electromechanical coupling is proportional to the dielectric constant, and whenever this constant is small in the matrix the effect of the fluctuations will be small too.

Particularly, we recall that Eshelby (1957) demonstrated that in composites with ellipsoidal inclusions the fields within the inclusions are uniform. Accordingly, from Eq. (3.40) it follows that in these cases the contribution to the Maxwell stress from fluctuations in the inclusions vanish. Moreover, if the dielectric moduli of the matrix phase is relatively small, the contribution from the fluctuations in the matrix phase will be relatively small too. Thus, we argue that for this class of composites the main contribution to the coupling is due to the jump in the intensity of the fields across the interfaces. We further note that in some cases the terms involving the field fluctuations vanish identically. For example, sequentially laminated composites (SLC) where a reasonable assumption is of piecewise constant fields within the phases (*e.g.*, Milton, 1986).

Once the second term in Eq. (3.40) is neglected, the following estimate for the constitutive relation between the macroscopic Maxwell stress and the applied electric field is obtained

$$\bar{\mathbf{T}}_M \cong \tilde{\mathbf{B}} : \bar{\mathbf{E}} \otimes \bar{\mathbf{E}}, \quad (3.41)$$

where, in indicial notation,

$$\tilde{B}_{ijkl} = \sum_{r=1}^n \lambda^{(r)} B_{mnpq}^{(r)} G_{mni}^{(r)} g_{pk}^{(r)} g_{ql}^{(r)}. \quad (3.42)$$

Here $\lambda^{(r)}$ is the volume fraction of the r -phase, and $\mathbf{g}^{(r)}$ and $\mathbf{G}^{(r)}$ are the electrostatic and elastic concentration tensors relating the overall fields to the average

fields in the phases such that

$$\begin{aligned}\bar{\mathbf{E}}^{(r)} &= \mathbf{g}^{(r)} \bar{\mathbf{E}}, \\ \bar{\boldsymbol{\varepsilon}}^{(r)} &= \mathbf{G}^{(r)} : \bar{\boldsymbol{\varepsilon}}.\end{aligned}\tag{3.43}$$

It is interesting to note that the form of the macroscopic constitutive relation (3.41) is reminiscent of the analogous local relation (3.11) for the homogeneous dielectrics.

We emphasize that the expressions for the concentration tensors $\mathbf{g}^{(r)}$ and $\mathbf{G}^{(r)}$ are derived from the *uncoupled* electrostatic and mechanical problems, respectively. As already mentioned, various results and estimates for the uncoupled homogenization problems are available in the literature. In view of Eq. (3.1) for $\bar{\mathbf{E}}$ and the corresponding expression for $\bar{\boldsymbol{\varepsilon}}$, the effective conductivity and elasticity tensors can be easily determined in terms of the concentration tensors. Moreover, for two-phase composites the concentration tensors can be extracted from the corresponding expressions for the effective moduli via the relations (Hill, 1963),

$$\mathbf{g}^{(r)} = \frac{1}{\lambda^{(r)}} (\mathbf{k}^{(r)} - \mathbf{k}^{(3-r)})^{-1} (\tilde{\mathbf{k}} - \mathbf{k}^{(3-r)}),\tag{3.44}$$

and

$$\mathbf{G}^{(r)} = \frac{1}{\lambda^{(r)}} (\mathbf{L}^{(r)} - \mathbf{L}^{(3-r)})^{-1} (\tilde{\mathbf{L}} - \mathbf{L}^{(3-r)}),\tag{3.45}$$

($r = 1, 2$).

3.3 Applications to specific composite classes

In the following Section we consider a few classes of composites for which explicit estimates for the macroscopic Maxwell stress can be determined. As appropriate for many cases of practical interest, we restrict our attention to planar loading condition as depicted in Fig. 2.2. Thus, we assume that the (x_1, x_2) -plane is the deformation plane and that the microstructure of the composite is fixed along the x_3 direction. Moreover, we note that due to the nature of the coupled phenomenon under consideration the number of parameters upon which the overall response of the composite depends is quite large. To somewhat reduce the number of independent parameters we restrict the following study to the class of incompressible

composites. We emphasize, however, that any of the following developments can be repeated for the broader class of compressible composites under spatial loading conditions. Finally, since in this Section we do not consider local fields fluctuations, for the sake of simplicity we drop the over-bar from quantities that represent averages over the phases.

3.3.1 Sequentially laminated composites

In this type of composites, due to the validity of the assumption of piecewise constant fields, the terms involving the fields fluctuations in Eq. (3.40) vanish, and an exact expression for the effective coupling tensor $\tilde{\mathbf{B}}$ of a rank- N SLC can be determined.

Consider a rank-1 laminate (see Fig. 3.1a) made out of two anisotropic phases with energy-density functions like in Eq. (3.28), in volume fractions $\lambda^{(i)}$ and $\lambda^{(m)} = 1 - \lambda^{(i)}$, respectively. Following the prescription described in Section 3.1.1, we can obtain explicit expressions for the electric and the strain concentration tensors in the form of Eqs. (3.43). However, in the limit of small deformations elasticity, the procedure is simpler. Thus, the expression for the macroscopic electromechanical coupling tensor $\tilde{\mathbf{B}}^{(\text{SLC})}$ can be obtained from Eq. (3.42).

First, we consider a rank-1 laminate made out of two isotropic and incompressible phases with dielectric moduli $k^{(m)}$ and $k^{(i)}$, and shear moduli $\mu^{(m)}$ and $\mu^{(i)}$. The volume fraction of the inclusions phase is $\lambda^{(i)}$. The principal axes of the effective dielectric and elastic tensors of this composite are collinear with the unit vectors normal and tangent to the interface. The principal effective dielectric and elastic moduli are the volume-averages and the harmonic volume-averages of the corresponding moduli of the phases (*e.g.*, deBotton and Hariton, 2002; Hariton and deBotton, 2003). The explicit expressions for the components of the effective coupling tensor $\tilde{\mathbf{B}}_{R1}^{(\text{SLC})}$ can be readily determined too. Specifically, when the laminate is subjected to an excitation field $\bar{\mathbf{E}} = E_0 \hat{\mathbf{x}}_2$ as demonstrated in Fig. 2.2, the components of the macroscopic Maxwell stresses in the principal coordinate

system are

$$\begin{aligned} T_{M\hat{n}\hat{n}} &= -T_{M\hat{m}\hat{m}} = \frac{\epsilon_0}{2} \left[\left(\frac{\lambda^{(m)}}{k^{(m)}} + \frac{\lambda^{(i)}}{k^{(i)}} \right)^{-1} \cos^2 \theta^{(1)} - (\lambda^{(m)}k^{(m)} + \lambda^{(i)}k^{(i)}) \sin^2 \theta^{(1)} \right] E_0^2, \\ T_{M\hat{m}\hat{n}} &= T_{M\hat{n}\hat{m}} = \epsilon_0 \left(\frac{\lambda^{(m)}}{k^{(m)}} + \frac{\lambda^{(i)}}{k^{(i)}} \right)^{-1} \cos \theta^{(1)} \sin \theta^{(1)} E_0^2, \end{aligned} \quad (3.46)$$

where $\theta^{(1)}$ is the lamination angle (see Fig. 3.1a). It turns out that in this particular case the macroscopic electromechanical stress is independent of the moduli $\mu^{(m)}$ and $\mu^{(i)}$. However, in more complicated microstructures \mathbf{T}_M does depend on the mechanical moduli.

Consider next a rank-2 laminate (Fig. 3.1b) consisting of layers of the former rank-1 laminate as the core phase together with layers of phase “ m ”. This is a particulate composite with isolated inclusions of phase “ i ” in a continuous matrix of phase “ m ”. However, the fields in the layers of the matrix phase in the core are different from those in the newly added layers of matrix phase. Henceforth these two distinct domains of the matrix phase will be treated as different phases. Similar to the procedure described in Section 3.1.1 we can determine the constants $\alpha^{(2)}$, $\omega^{(2)}$ and the effective dielectric and elastic tensors. From Eq. (3.44) we determine three concentration tensors that relate the three different electric fields in the composite with $\bar{\mathbf{E}}$ (*i.e.*, the fields in the inclusion phase, in the matrix phase in the core, and in the newly added matrix layers). In analogy with Eq. (3.45), the three concentration tensors relating the strains in the three domains with $\bar{\boldsymbol{\epsilon}}$ are determined too. Finally, an explicit expression for the corresponding macroscopic electromechanical coupling tensor $\tilde{\mathbf{B}}_{R2}^{(SLC)}$ is determined via Eq. (3.42).

We recall that with an appropriate choice of the phases volume fractions and lamination directions the effective mechanical properties of an incompressible rank-2 composite can become transversely isotropic. The transverse isotropic plane is spanned by the two normals to the lamination directions (*i.e.*, the (x_1, x_2) -plane in Fig. 3.1b). It is further possible to construct the composite such that its effective properties attain the Hashin-Shtrikman bounds (Francfort and Murat, 1986). Particularly, if we choose the softer phase as the matrix phase this special

microstructure attains the Hashin-Shtrikman lower bound, ensuring that its elastic modulus is the smallest possible. This special material is constructed with an angle $\alpha = \pi/4$ between the two lamination directions of the rank-2 composite (see Fig. 3.1b). The effective shear moduli in the transverse plane is

$$\tilde{\mu}_T^{(R2)} = \mu^{(m)} \frac{(1 - \lambda^{(i)}) \mu^{(m)} + (1 + \lambda^{(i)}) \mu^{(i)}}{(1 + \lambda^{(i)}) \mu^{(m)} + (1 - \lambda^{(i)}) \mu^{(i)}}. \quad (3.47)$$

We also note that the composite's dielectric tensor is not isotropic and its orientation can be chosen to enhance or reduce the electromechanical coupling.

By iterative application of the above procedure the effective electric and elastic moduli, together with the macroscopic electromechanical coupling tensor of sequentially laminated composites can be determined. The rank-6 laminate with internal lamination angles $\alpha = \pi/3$ is an interesting case. With an appropriate choice of the laminates volume fractions, both the elastic and the dielectric tensors admit plane isotropy (transverse isotropy) (Milton, 2002; deBotton, 2005). Moreover, the properties of this microstructure are extremal in the sense that they attain the Hashin-Shtrikman bounds for the class of transversely isotropic composites (Francfort and Murat, 1986). Thus, the expression for the effective transverse shear moduli is identical to the one given in Eq. (3.47) (*i.e.*, $\tilde{\mu}_T^{(R6)} = \tilde{\mu}_T^{(R2)}$). The expression for the effective in-plane dielectric modulus $\tilde{k}_T^{(R6)}$ is also identical to the expression given in Eq. (3.47), but with $k^{(m)}$ and $k^{(i)}$ instead of $\mu^{(m)}$ and $\mu^{(i)}$, respectively. However, within the context of the present work, we find it interesting that the overall electromechanical response of this extremal composite is isotropic too (in the transverse plane).

3.3.2 Hashin-Shtrikman estimates

We examine the electromechanical coupling in the transverse plane of two-phase fiber composites. To this end we use the expressions developed by Willis (1977, 1981) for the HS bounds on the overall dielectric and elastic moduli to extract corresponding HS estimates for the macroscopic electromechanical coupling. We recall that Milton and Kohn (1988) showed that in optimal composites attaining the Hashin-Shtrikman bounds the fields are uniform in one of the phases. In

these microstructures the lower HS bound is attained when the phase with the lower moduli serves as the matrix phase (and vice versa for the upper bound). Accordingly, the above mentioned arguments in favor of using Eq. (3.42) as an estimate for the effective coupling tensor hold in this case too. In the sequel we present examples that demonstrate that these provide fine estimates for the overall electromechanical coupling in composites with hexagonal unit cell.

Following Willis (1977), the concentration tensors of fiber composites with isotropic fibers in volume fraction $\lambda^{(i)}$ in a isotropic matrix with $\lambda^{(m)} = 1 - \lambda^{(i)}$ are

$$\begin{aligned} \mathbf{g}_{HS}^{(r)} &= [\mathbf{I} + \mathbf{P}_k (\mathbf{k}^{(r)} - \mathbf{k}^{(0)})]^{-1} \left\{ \sum_{s=1}^2 \lambda^{(s)} [\mathbf{I} + \mathbf{P}_k (\mathbf{k}^{(s)} - \mathbf{k}^{(0)})]^{-1} \right\}^{-1}, \\ \mathbf{G}_{HS}^{(r)} &= [\mathfrak{J} + \mathbf{P}_L (\mathbf{L}^{(r)} - \mathbf{L}^{(0)})]^{-1} \left\{ \sum_{s=1}^2 \lambda^{(s)} [\mathfrak{J} + \mathbf{P}_L (\mathbf{L}^{(s)} - \mathbf{L}^{(0)})]^{-1} \right\}^{-1}, \end{aligned} \quad (3.48)$$

where $\mathfrak{J}_{ijkl} = \frac{1}{2} (\delta_{ik}\delta_{jl} + \delta_{il}\delta_{jk})$ is the fourth-order ‘‘unit’’ tensor, \mathbf{P}_k and \mathbf{P}_L are constant tensors, and the superscript ‘‘0’’ represents a comparison material. Eshelby (1957) presented the tensor S_{ijkl} (which is frequently denoted ‘‘Eshelby’s tensor’’) for the elastic problem of an ellipsoidal inclusion. This tensor is expressed in terms of elliptic integrals and is related to the constant tensor \mathbf{P}_L by

$$\mathbf{P}_L = \mathbf{S} (\mathbf{L}^{(0)})^{-1}. \quad (3.49)$$

In a similar manner, for the corresponding electrostatic problem, one can determine a tensor s_{ij} such that

$$\mathbf{P}_k = \mathbf{s} (\mathbf{k}^{(0)})^{-1}. \quad (3.50)$$

We recall that in the literature there are works in which an explicit expression for Eshelby’s tensor is given. In these works, various shapes and spatial distributions of the inclusion were considered. Here we consider randomly-dispersed fiber composites with two types of the inclusion’s cross section, a circular and an elliptic (as shown in Fig. 3.4). Materials with the first type of fibers belong to the class of transversely isotropic composites, and composites with the second type of fibers admit orthotropic symmetry.

Transversely isotropic fiber composites

An efficient notation for representing the properties of materials admitting transversely isotropic symmetry was introduced by Walpole (1969). In this notation the elastic and dielectric tensors are expressed in the form (details are given in Appendix A)

$$\begin{aligned}\mathbf{k}^{(r)} &= \left(k_L^{(r)}, k_T^{(r)} \right), \\ \mathbf{L}^{(r)} &= \left(2\kappa_T^{(r)}, l^{(r)}, l^{(r)}, n^{(r)}, 2\mu_T^{(r)}, 2\mu_L^{(r)} \right).\end{aligned}\quad (3.51)$$

Here k_L and k_T are the longitudinal and transverse dielectric moduli, respectively, κ_T is the transverse plane-strain dilatational modulus, n is the longitudinal uniaxial straining modulus, l is the cross-modulus, μ_T is the transverse shear modulus and μ_L is the longitudinal shear modulus. For an isotropic material these relations can be used with $k_L = k_T = k$, $\kappa_T = K + 1/3\mu$, $l = K - 2/3\mu$, $n = K + 4/3\mu$ and $\mu_T = \mu_L = \mu$, where K is the bulk modulus. Following Walpole's notation the electromechanical coupling tensor (defined in Eq. (3.12)) for a homogeneous transversely isotropic dielectric can be expressed as

$$\mathbf{B}^{(r)} = \epsilon_0 \left(k_T^{(r)} - 1, -\frac{1}{2}, -\frac{1}{2}, k_L^{(r)} - \frac{1}{2}, k_T^{(r)}, \frac{1}{2} \left(k_L^{(r)} + k_T^{(r)} \right) \right). \quad (3.52)$$

We note that under planar loading only the first and the fifth terms in Eq. (3.52) are relevant.

Following Willis (1981), the constant tensors (in Walpole's notation) in Eq. (3.48) corresponding to the HS bounds on the dielectric and the elastic moduli of transversely isotropic fiber composites are

$$\begin{aligned}\mathbf{P}_k^{(\text{TI})} &= \left(0, \frac{1}{2k^{(0)}} \right), \\ \mathbf{P}_L^{(\text{TI})} &= \left(\frac{1}{2(l^{(0)} + 2\mu^{(0)})}, 0, 0, 0, \frac{l^{(0)} + 3\mu^{(0)}}{4\mu^{(0)}(l^{(0)} + 2\mu^{(0)})}, \frac{1}{4\mu^{(0)}} \right).\end{aligned}\quad (3.53)$$

By choosing the properties of the comparison material (phase "0" in Eq. (3.48)) equal to those of the phase with the lower dielectric and elastic moduli, the following Hashin-Shtrikman lower bounds on the corresponding effective dielectric and

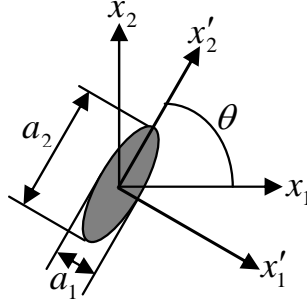


Fig. 3.4: Schematic drawing of fiber with elliptic cross-section.

elastic moduli are obtained

$$\begin{aligned}\tilde{\mathbf{k}}^{(\text{TI})} &= (\tilde{k}_L, \tilde{k}_T), \\ \tilde{\mathbf{L}}^{(\text{TI})} &= (2\tilde{\kappa}_T, \tilde{l}, \tilde{n}, 2\tilde{\mu}_T, 2\tilde{\mu}_L).\end{aligned}\tag{3.54}$$

Here \tilde{k}_L is the volume-average of the phases' dielectric moduli, and the expression for \tilde{k}_T , which is identical to the expression for $\tilde{k}_T^{(\text{R6})}$, was obtained by Hashin (1970). The expressions for the five effective elastic moduli were derived by Hashin and Rosen (1964), Hill (1964) and Hashin (1965). For the class of incompressible fiber composites subjected to planar loading in the transverse plane the only relevant modulus is the transverse shear modulus $\tilde{\mu}_T$. The expression for this modulus is identical to the one for $\tilde{\mu}_T^{(\text{R2})}$ in Eq. (3.47). Finally, the expressions for the two relevant coefficients of the macroscopic electromechanical coupling tensor $\tilde{\mathbf{B}}_{TI}^{(\text{HS})}$ are

$$\begin{aligned}\tilde{B}_{TI1}^{(\text{HS})} &= \epsilon_0 \frac{(k^{(m)} - 1) (k^{(m)} + k^{(i)})^2}{[(1 + \lambda^{(i)}) k^{(m)} + (1 - \lambda^{(i)}) k^{(i)}]^2}, \\ \tilde{B}_{TI5}^{(\text{HS})} &= \epsilon_0 \frac{k^{(m)} \left[(1 - \lambda^{(i)}) (k^{(m)} + k^{(i)})^2 (\mu^{(m)} + \mu^{(i)}) + 8\lambda^{(i)} k^{(m)} k^{(i)} \mu^{(m)} \right]}{[(1 + \lambda^{(i)}) k^{(m)} + (1 - \lambda^{(i)}) k^{(i)}]^2 [(1 + \lambda^{(i)}) \mu^{(m)} + (1 - \lambda^{(i)}) \mu^{(i)}]}.\end{aligned}\tag{3.55}$$

Orthotropic fiber composites

We consider the class of composites with fibers with elliptic cross section (ECS) monotonically aligned in a isotropic matrix in x_3 direction. The aspect ratio of the cross section is $\gamma \equiv a_1/a_2 < 1$ (see Fig. 3.4). We assume that the fibers are randomly-dispersed in the transverse plane and that their principal axes parallel

so that the material as a whole is orthotropic (with respect to the principal axes x'_1 - x'_2 of the elliptic cross section in Fig. 3.4). Eshelby's tensors (*e.g.*, Duan et al., 2006; Zhao and Weng, 1990, for the corresponding uncoupled electric and elastic problems, respectively) can be expressed in terms of the aspect ratio γ and the Poisson's ratio of the comparison material $\nu^{(0)}$

$$\mathbf{s}^{(\text{ECS})} = \begin{pmatrix} \frac{1}{1+\gamma} & 0 & 0 \\ 0 & \frac{\gamma}{1+\gamma} & 0 \\ 0 & 0 & 0 \end{pmatrix}, \quad (3.56)$$

and

$$\mathbf{S}^{(\text{ECS})} = \begin{pmatrix} S_{11} & S_{12} & S_{13} & 0 & 0 & 0 \\ S_{21} & S_{22} & S_{23} & 0 & 0 & 0 \\ S_{31} & S_{32} & S_{33} & 0 & 0 & 0 \\ 0 & 0 & 0 & S_{44} & 0 & 0 \\ 0 & 0 & 0 & 0 & S_{55} & 0 \\ 0 & 0 & 0 & 0 & 0 & S_{66} \end{pmatrix}, \quad (3.57)$$

where

$$S_{11} = \frac{1}{2(1-\nu^{(0)})} \left[\frac{1+2\gamma}{(1+\gamma)^2} + \frac{1-2\nu^{(0)}}{1+\gamma} \right],$$

$$S_{12} = \frac{1}{2(1-\nu^{(0)})} \left[\frac{1}{(1+\gamma)^2} + \frac{1-2\nu^{(0)}}{1+\gamma} \right],$$

$$S_{13} = \frac{\nu^{(0)}}{1-\nu^{(0)}} \frac{1}{1+\gamma},$$

$$S_{21} = \frac{\gamma}{2(1-\nu^{(0)})} \left[\frac{\gamma}{(1+\gamma)^2} - \frac{1-2\nu^{(0)}}{1+\gamma} \right],$$

$$S_{22} = \frac{\gamma}{2(1-\nu^{(0)})} \left[\frac{\gamma+2}{(1+\gamma)^2} + \frac{1-2\nu^{(0)}}{1+\gamma} \right],$$

$$S_{23} = \frac{\nu^{(0)}}{1-\nu^{(0)}} \frac{\gamma}{1+\gamma},$$

$$S_{31} = S_{32} = S_{33} = 0,$$

$$S_{44} = \frac{\gamma}{2(1+\gamma)},$$

$$S_{55} = \frac{1}{2(1+\gamma)},$$

$$S_{66} = \frac{1}{4(1 - \nu^{(0)})} \left[\frac{1 + \gamma^2}{(1 + \gamma)^2} + (1 - 2\nu^{(0)}) \right].$$

By substituting Eqs. (3.56) and (3.57) in Eqs. (3.50) and (3.49), respectively, the constant tensors $\mathbf{P}_k^{(\text{ECS})}$ and $\mathbf{P}_L^{(\text{ECS})}$ in Eq. (3.48) can be determined. Next, with the aid of Eq. (3.42) we can extract the expression for the macroscopic coupling tensor $\tilde{\mathbf{B}}_{ECS}^{(\text{HS})}$. We note that in the limit when the elliptic cross section becomes a circular one (*i.e.*, $\gamma = 1$) we recover the result for the transversely isotropic composite $\tilde{\mathbf{B}}_{TI}^{(\text{HS})}$. In the other limit, of penny-shaped inclusions (*i.e.*, $\gamma \rightarrow 0$) the result for the rank-1 laminated composite $\tilde{\mathbf{B}}_{R1}^{(\text{SLC})}$ is recovered.

3.3.3 Third order estimates

The well known bounds of Hashin and Shtrikman (1962) on the effective properties of composites depend on two-point correlation function. It is possible to improve the estimates for the electromechanical coupling by using additional information about the composite. In particular, third order bounds incorporate high order correlation functions that provide statistical information about the composite's microstructure (*e.g.*, Torquato, 1991, and references therein). Beran (1965) introduced bounds on the effective conductivity of three-dimensional isotropic media involving three-point probability functions. These bounds depend on a second geometrical parameter (in addition to the volume fraction).

Milton (1981, 1982) demonstrated later that the same parameter arises in bounds on the effective bulk modulus of two-phase isotropic composites. Three-point bounds on the effective shear modulus further depend on an additional parameter (Milton, 1982). Gibiansky and Torquato (1995) reviewed various bounds on the effective conductivity and elastic moduli of two-phase isotropic composites that depend on geometrical parameters that take into account up to three-point statistical information. They applied a special transformation to express these bounds in a new and convenient form. More recently Berryman (2006) compared various methods for utilizing improved bounds and microstructural correlation information in a useful way for estimating material constants in heterogeneous media.

Torquato and Lado (1992) evaluated improved bounds on the effective moduli of transversely isotropic composites with aligned, infinitely long, fibers with circular cross section distributed throughout a matrix. Since in this work we are considering the class of incompressible composites subjected to planar loading, only the in-plane moduli (dielectric and shear) are relevant. The bounds on the transverse dielectric modulus are

$$k_T^{(3OB-L)} \leq \tilde{k}_T \leq k_T^{(3OB-U)},$$

where

$$k_T^{(3OB-U)} = \left[\langle k \rangle - \frac{\lambda^{(1)}\lambda^{(2)}(k^{(2)} - k^{(1)})^2}{\langle \check{k} \rangle + \langle k \rangle_\zeta} \right], \quad (3.58)$$

$$k_T^{(3OB-L)} = \left[\langle 1/k \rangle - \frac{\lambda^{(1)}\lambda^{(2)}(1/k^{(2)} - 1/k^{(1)})^2}{\langle \check{1/k} \rangle + \langle 1/k \rangle_\zeta} \right]^{-1}, \quad (3.59)$$

and the bounds on transverse shear modulus are

$$\mu_T^{(3OB-L)} \leq \tilde{\mu}_T \leq \mu_T^{(3OB-U)}$$

where

$$\mu_T^{(3OB-U)} = \left[\langle \mu \rangle - \frac{\lambda^{(1)}\lambda^{(2)}(\mu^{(2)} - \mu^{(1)})^2}{\langle \check{\mu} \rangle + \Theta} \right], \quad (3.60)$$

$$\mu_T^{(3OB-L)} = \left[\langle 1/\mu \rangle - \frac{\lambda^{(1)}\lambda^{(2)}(1/\mu^{(2)} - 1/\mu^{(1)})^2}{\langle \check{1/\mu} \rangle + \Xi} \right]^{-1}, \quad (3.61)$$

$$\Theta = \left[2 \langle \kappa_T \rangle_\zeta \langle \mu \rangle^2 + \langle \kappa_T \rangle^2 \langle \mu \rangle_\eta \right] / \langle \kappa_T + 2\mu \rangle^2, \quad (3.62)$$

$$\Xi = 2 \langle 1/\kappa_T \rangle_\zeta + \langle 1/\mu \rangle_\eta. \quad (3.63)$$

In the above relations $\langle a \rangle = \lambda^{(1)}a^{(1)} + \lambda^{(2)}a^{(2)}$, $\langle \check{a} \rangle = \lambda^{(2)}a^{(1)} + \lambda^{(1)}a^{(2)}$ and $\langle a \rangle_{(\bullet)} = (\bullet)^{(1)}a^{(1)} + (\bullet)^{(2)}a^{(2)}$, where $\zeta^{(1)} = 1 - \zeta^{(2)}$ and $\eta^{(1)} = 1 - \eta^{(2)}$ are the geometrical or microstructural parameters. Torquato and Lado (1992) demonstrate that since the values of the parameters $\zeta^{(r)}$ and $\eta^{(r)}$ are in the interval $[0, 1]$, the above third-order bounds are always between the second-order bounds of Hill (1964) and Hashin (1965). They further found that for the class of composites with random array of

impenetrable fibers in volume fraction $0 \leq \lambda^{(2)} \leq 0.7$ accurate estimates for the microstructural parameters are

$$\zeta^{(2)} = \frac{\lambda^{(2)}}{3} - 0.05707 (\lambda^{(2)})^2 \quad (3.64)$$

and

$$\eta^{(2)} = \frac{56}{81} \lambda^{(2)} + 0.0428 (\lambda^{(2)})^2. \quad (3.65)$$

Once the third-order bounds $\tilde{\mathbf{k}}^{(3OB)}$ and $\tilde{\mathbf{L}}^{(3OB)}$ are determined, from Eqs. (3.44) and (3.45) the dielectric and elastic concentration tensors $\mathbf{g}_{3OB}^{(r)}$ and $\mathbf{G}_{3OB}^{(r)}$ ($r = 1, 2$), can be extracted. Finally, from Eq. (3.42) an estimate for the third-order macroscopic coupling tensor $\tilde{\mathbf{B}}_{TI}^{(3OE)}$ is obtained.

3.3.4 Periodic composites with hexagonal unit cell

The class of fiber composites with hexagonal unit cell (see Fig. 4.4) is frequently used as an idealized model for fiber composites with periodic microstructures. In the limit of infinitesimal deformations the response of linear elastic composites belonging to this class is transversely isotropic. Moreover, the macroscopic electrostatic and elastic responses of the composite are very similar to those of the transversely isotropic rank-6 laminate and hence also to the HS bounds. In this respect, a comparison of the coupled electromechanical response of this composite with the corresponding analytical estimates will highlight the contribution of the microstructure to the coupling.

The simplicity of the unit cell representing this microstructure makes it an ideal candidate for finite element simulations. In this work the numerical simulations are determined by application of an external procedure in conjunction with the commercial FE code ABAQUS and a set of periodic boundary conditions. Further details concerning the numerical simulations and the appropriate boundary conditions are given in Chapter 4.

The similarity between the uncoupled responses of the periodic composite and the estimates considered in the previous Subsections is demonstrated in Fig. 3.5. Shown are the variations of the effective in-plane dielectric and shear moduli

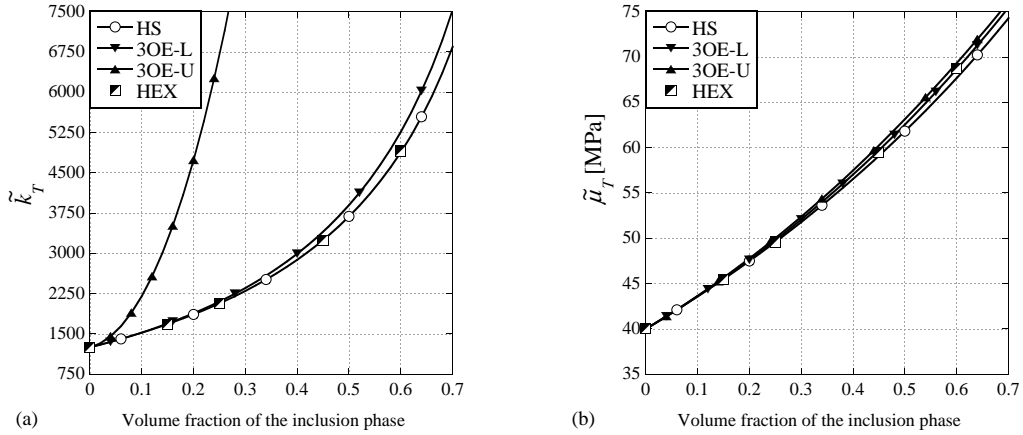


Fig. 3.5: Effective properties of incompressible dielectric composites with hexagonal unit cell and corresponding HS lower bounds and third-order bounds on the transverse (a) dielectric and (b) shear moduli.

of composites with hexagonal unit cell and with volume fractions of the inclusion phase $\lambda^{(i)} = 0.15, 0.25, 0.45$ and 0.6 (black and white squares). The properties of the matrix phase are reminiscent of those for the barium titanate ceramic *i.e.*, $\mu^{(m)} = 40$ [MPa] and $k^{(m)} = 1250$ and the properties of the inclusion phase are representative of a stiffer conducting material with $\mu^{(i)} = 100$ [MPa] and $k^{(i)} = 200,000$. For both materials the bulk modulus assumed in the numerical simulations is $\kappa \approx 500\mu$, ensuring negligible volumetric deformations of the composite.

The numerical simulations are compared with corresponding HS lower bounds and third-order bounds for incompressible transversely isotropic composites. These are determined by application of Eqs. (3.54), (3.47) and (3.58)-(3.61). Indeed, the effective properties of the periodic composites are very close to the HS and third-order lower bounds (and hence also to those of the incompressible rank-6 laminated composite).

3.3.5 A “naive” estimate

We conclude this Subsection noting that an extremely simple estimate for the macroscopic coupling is obtained by treating the composite as a homogenized elas-

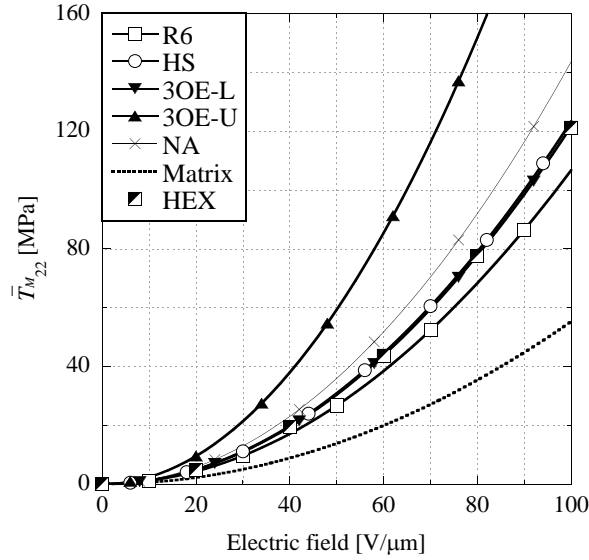


Fig. 3.6: The Maxwell stresses developing in a rank-6 sequentially laminated composite and a composite with hexagonal unit cell, shown together with corresponding HS, third-order and naive estimates as functions of the electric excitation. The inclusion volume fraction is $\lambda^{(i)} = 0.45$. The dashed curve corresponds to the behavior of the matrix phase.

tic dielectric. Thus, the effective dielectric tensor of the composite $\tilde{\mathbf{k}}$ is determined and substituted instead of $\mathbf{k}^{(r)}$ in Eq. (3.12) to end up with an estimate for the macroscopic coupling tensor. In the sequel we denote this estimate $\tilde{\mathbf{B}}^{(\text{NA})}$ and, for the lack of a better name, refer to it as the “naive” estimate. We note that any type of estimate for the effective dielectric moduli of the composite can be utilized for determining the naive estimate. In the next Section we will choose the HS lower bound to this end.

3.3.6 Examples

In this Subsection we examine the overall electromechanical response of heterogeneous elastic dielectrics with the aid of specific numerical examples. These serve to highlight the role of micromechanical parameters such as volume fraction and phases properties on the overall macroscopic response. The role of the spatial arrangement of the phases is highlighted through a comparison between the re-

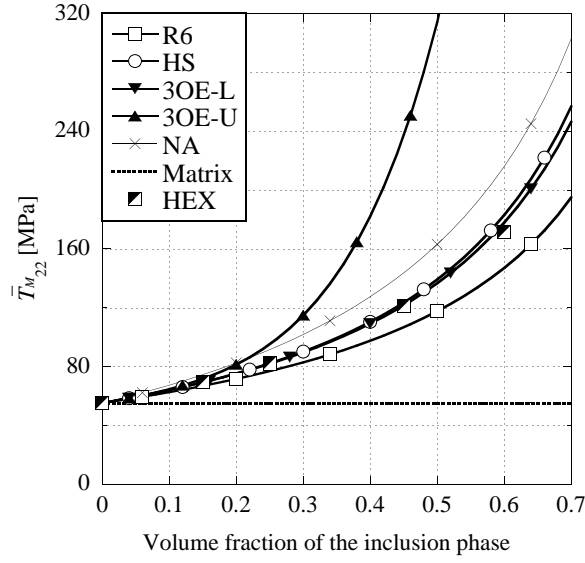


Fig. 3.7: The Maxwell stress as a function of the inclusions volume fraction. Results for rank-6 composites, FE simulations of periodic composites and HS, third-order and naive estimates. The dashed curve corresponds to the stress in the matrix phase.

sponses predicted by the different composites.

Initially we track the evolution of the macroscopic Maxwell stress of composites with softer matrix and stiffer conducting inclusions. The composites are subjected to “electrostatic loading” as in Section 3.2, and the properties of the two constituents are those considered in Subsection 3.3.4. Shown in Fig. 3.6 are the variations of the normal component of the Maxwell stresses developing between the electrodes (\bar{T}_{M22}) as functions of the excitation electric field \bar{E}_2 (e.g., Fig. 2.2). The curve marked by clear squares corresponds to the rank-6 composite, the one for the HS estimate is marked by clear circles, the curves for the third-order estimates are marked with upright and inverted triangles, and the one for the naive approximation by the cross marks. Here and throughout this Section the HS lower bound was chosen for determining the effective dielectric modulus required for the naive estimate. The FE results for the periodic composite with hexagonal unit cell are marked by black and white squares. The volume fraction of the inclusions phase is 0.45. For comparison, the dashed curve shows the Maxwell stress that would develop in the matrix due to similar electric excitation.

As it should, the dependency of the Maxwell stress on the applied electric field is quadratic. We observe that the macroscopic Maxwell stress in the rank-6 composite is lower than the one in the hexagonal cell composite. The curves for the HS and the third-order lower estimates coincide with the numerical results for the periodic composite. The naive approximation and the third-order upper estimate overestimate the results for the two composites. An important observation concerns the intensity of the stresses. For an excitation field of $100[\text{V}/\mu\text{m}]$, the Maxwell stress in the matrix phase is approximately $60[\text{MPa}]$ and in the composites is about $120[\text{MPa}]$. These stresses are not negligible and may result in mechanical failure.

In Fig. 3.7 we examine the effect of the inclusions volume fraction on the macroscopic Maxwell stress for a fixed excitation field $\bar{E}_2 = 100[\text{V}/\mu\text{m}]$. The caption is identical to the one in Fig. 3.6. In a manner similar to the one observed in the previous plot, the results for the rank-6 composite are beneath the FE simulations, while the curves for the HS estimate and the third-order lower estimate are in agreement with the FE results. Once again the naive approximation, which neglects the internal mechanical interaction between the phases, and the third-order upper estimate overestimate the magnitude of the stresses in the periodic composite. We recall that in the composites we examine, the inclusion phase is both stiffer and has a higher dielectric constant. In this respect the growth of the macroscopic stress as the volume fraction of the inclusion phase increases is anticipated.

Variations of the Maxwell stress as functions of the contrast between the dielectric moduli of the phases are depicted in Fig. 3.8 for composites with $\lambda^{(i)} = 0.45$. The order in which the curves are organized is identical to the one in the previous two plots. The rank-6 laminates admit weaker electromechanical coupling than the periodic composites, and the HS estimate neatly approximates the numerical results. The third-order lower estimate also captures the composites' response, and the third-order upper estimate overestimates them. The naive approximation progressively worsens as the contrast increases. We note, however, that beyond a contrast of about 20 between the moduli, the rate of growth of the macroscopic

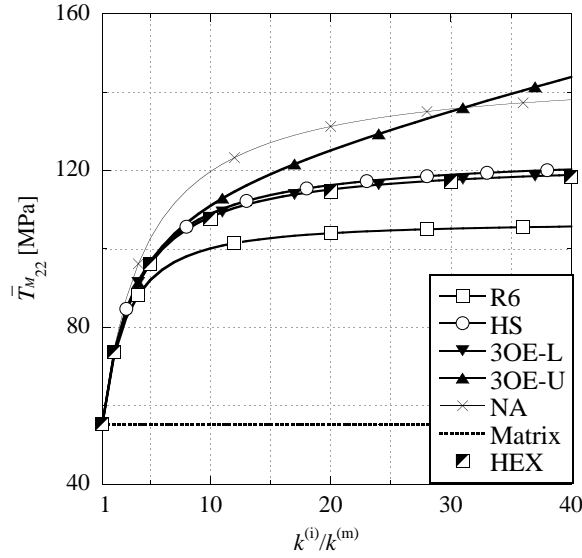


Fig. 3.8: The macroscopic Maxwell stress as function of the contrast between the phases' dielectric constants for rank-6 composites, HS estimates, third-order estimates, naive estimates and FEM simulations of periodic composites, all with $\lambda^{(i)} = 0.45$.

stress becomes small. Thus, only a limited improvement in the electromechanical coupling may be achieved by means of increasing the dielectric modulus of the inclusions.

Next, we wish to highlight the effect of the microstructure on the overall response of the composite. To this end we note that when the boundary of a homogeneous elastic dielectric is traction free, the strains developing due to electrostatic loading depend on both its dielectric and elastic moduli via the relation $\boldsymbol{\varepsilon} = \mathbf{L}^{-1}\mathbf{B} : \mathbf{E} \otimes \mathbf{E}$. Particularly, for incompressible isotropic dielectrics these strains depend on the ratio between the dielectric and the shear moduli. Thus, under similar electrostatic boundary conditions two different materials exhibit the same strain response if the ratio between these two moduli is the same for both materials (as was demonstrated in Fig. 3.3). Here we exploit this observation and consider the class of composites whose phases have identical strain response. Clearly, any differences between the macroscopic strains in the composites and those that would develop in the phases are due to the heterogeneity and depend solely on the spatial arrangement of the phases.

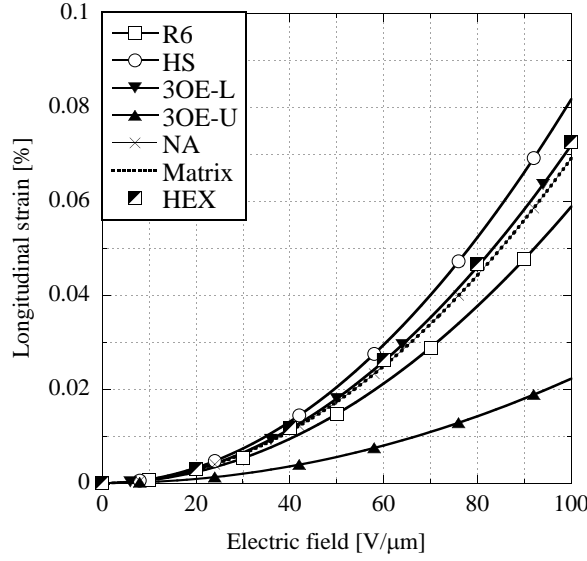


Fig. 3.9: The actuation strains of a rank-6 sequentially laminated composite and a composite with hexagonal unit cell shown together with corresponding HS, third-order and naive estimates as functions of the electric excitation. The inclusions' volume fraction is $\lambda^{(i)} = 0.45$. The dashed curve corresponds to the behavior of the matrix phase.

The actuation strains ($\bar{\varepsilon}_{11}$ in Fig. 2.2) as functions of the exciting electric field in composites with phases having the same electromechanical strain response are shown in Fig. 3.9. Specifically, the properties of the matrix phase are $\mu^{(m)} = 40[\text{MPa}]$ and $k^{(m)} = 1250$ (as in the previous plots), and the dielectric and shear moduli of the inclusion phase are $\mu^{(i)} = 1600[\text{MPa}]$ and $k^{(i)} = 50000$, respectively. The inclusions' volume fraction is 0.45. The caption in this plot is identical to the one in the previous ones.

Clearly, since the electromechanical coupling in the matrix and the inclusion are identical, the dashed curve in the plot corresponds to the behaviors of both the matrix and the inclusion. Due to the spatial arrangements of the phases the overall strain developing in the rank-6 laminate is lower than the ones that would develop in the homogeneous phases. Contrarily, in the periodic composite the microstructure results in a slight amplification of the actuation strains. Here too the third-order lower estimate agrees with the finite element results for the hexagonal composite and the HS estimate slightly overestimates them. Finally, for

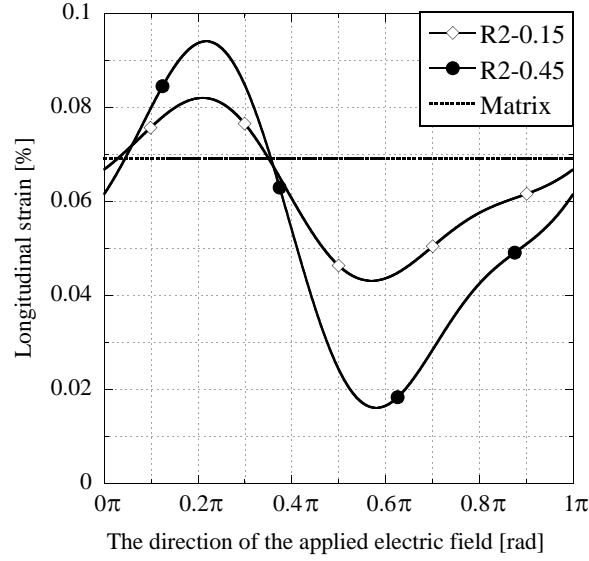


Fig. 3.10: Actuation strains of rank-2 laminated composites with $\lambda^{(i)} = 0.15$ and 0.45 as functions of the direction of the applied electric field.

consistency with the choice of the effective dielectric modulus for the naive estimate we chose the HS lower bound on the shear modulus as the corresponding estimate for determining the associated actuation strain. Since the expressions for the HS lower bounds on the dielectric and the shear moduli are identical, the actuation strain predicted by the naive estimate is identical to the actuation strains of the individual constituents.

To further examine the influence of the microstructure on the overall electro-mechanical coupling we consider next a rank-2 laminated composite made out of two-phases with identical strain response. In this composite the microstructure is such that the overall mechanical response is isotropic (in the deformation plane) while the dielectric tensor is anisotropic. Consequently, in this composite the actuation strain normal to the direction of the applied electric field will vary with the direction of the applied field relative to the lamination angle ($\theta^{(2)}$ in Fig. 3.1b). Shown in Fig. 3.10 are the actuation strains of two rank-2 composites as functions of the direction of the applied electric field. The curves marked by diamonds and circles are for composites with $\lambda^{(i)} = 0.15$ and 0.45 , respectively. The dashed curve shows the strain responses of the matrix and the inclusion phases under similar

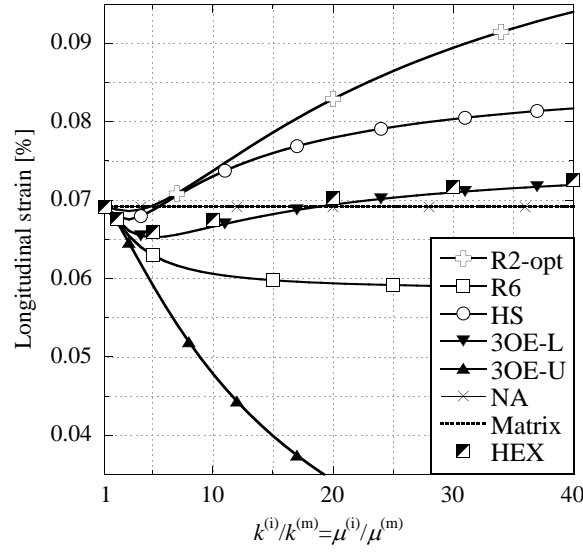


Fig. 3.11: Actuation strains of rank-2 composites along the direction where the electromechanical coupling is maximized as functions of the contrast between the moduli of the phases. Also shown are the corresponding strains of rank-6 composites, hexagonal cell composites, and the HS, third-order and the naive estimates. The inclusions' volume fraction is $\lambda^{(i)} = 0.45$. The dashed curve shows the response of the homogeneous phases.

excitation electric field ($100[\text{V}/\mu\text{m}]$). The pronounced dependency of the strain on the direction of the applied field can be appreciated. Particularly, along the direction where the response of the composite is maximized ($\theta^{(2)} \sim 0.2\pi$), the electromechanical coupling is amplified by 35% for the composite with $\lambda^{(i)} = 0.45$. Along the direction where the coupling is minimized ($\theta^{(2)} \sim 0.6\pi$), there is almost 80% attenuation. We emphasize that these marked differences are solely due to the variations in the microstructure since the strain responses of the phases are identical.

Finally, we examine the influence of the contrast between the properties of the two-phases on the electromechanical response of the composites. Shown in Fig. 3.11 are the actuation strains of rank-2 laminates along the direction where the strains are maximized as functions of the contrast between moduli of the phases (*i.e.*, $k^{(i)}/k^{(m)} = \mu^{(i)}/\mu^{(m)}$). These are compared with the strains of the rank-6 composites, the hexagonal cell composites, and the HS, the third-order and the

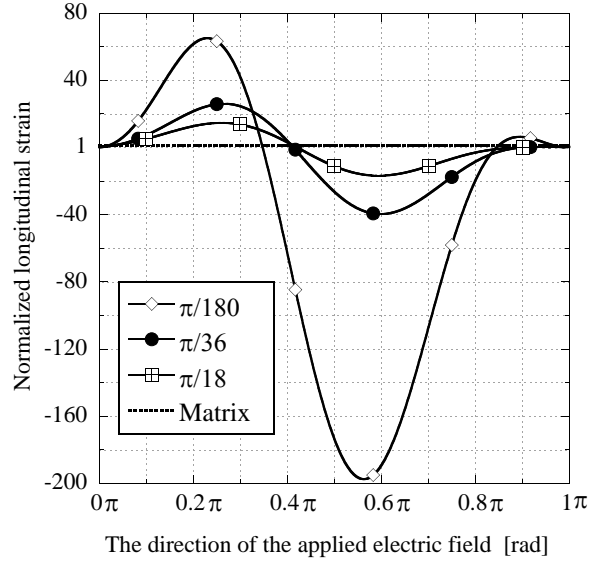


Fig. 3.12: Longitudinal strains of rank-2 laminated composites with $\lambda^{(z)} = 0.30$ as functions of the direction of the applied electric field for a few fixed lamination angles. These are normalized by the response of the matrix phase (the dashed curve).

naive estimates for the transversely isotropic composites.

Interestingly, according to all models but the rank-6 composites and the third-order upper estimates, when the contrast is small the coupling in the composites are weaker than the coupling in the phases. However, in composites with higher contrast the electromechanical coupling in the composites is stronger. Along the chosen direction the actuation strains of the anisotropic rank-2 composites are markedly larger than those determined for the transversely isotropic composites. The curve for the third-order lower estimates closely follows the one for the periodic hexagonal composites, while the HS curve overestimates the numerical results. As before, the coupling in the rank-6 composites is the weakest. The curve for the naive estimate lies on top of the dashed curve for the homogeneous phases.

3.4 Optimization

The availability of analytical expressions for the behavior of EAPCs enables to execute optimization procedures in a straightforward manner. The purpose is to reveal the best possible microstructure that will provide maximal actuation under

given boundary conditions (*e.g.*, Fig. 2.2). The analytical estimates of Section 3.3 are used to design a model with an optimal microstructure for given volume fraction and phases' properties. To this end, we consider only the anisotropic composites (*e.g.*, sequentially laminated and orthotropic fiber composites). In fact, we focus on two simple microstructures, the rank-2 laminated composites and the class of composites with fibers with elliptic cross section. This optimization process can be repeated for other composite types and microstructures.

3.4.1 Rank-2 laminated composites

We consider rank-2 laminated composites (see Fig. 3.1b) with inclusions' volume fraction

$$\lambda^{(i)} = \lambda^{(1)}\lambda^{(2)} = 0.30, \quad (3.66)$$

where $\lambda^{(1)} = 0.40$ is the volume fraction of the inclusion phase in the inner rank-1 and $\lambda^{(2)} = 0.75$ is the volume fraction of the core (rank-1) in the rank-2 material.

Initially we track the coupling response of rank-2 laminated composites with softer matrix and stiffer conducting inclusions with $k^{(i)}/k^{(m)} = 10^5$ and $\mu^{(i)}/\mu^{(m)} = 70$. Shown in Fig. 3.12 are the variations of the longitudinal strains as functions of the direction of the applied electric field for a fixed lamination angle ($\theta^{(2)}$ and α in Fig. 3.1b, respectively). To highlight the role of the microstructure we normalized the macroscopic longitudinal strain by that of the matrix phase under similar loading conditions (*i.e.*, $\bar{\varepsilon}_{11}/\varepsilon_{11}^{(m)}$). The curves marked by clear diamonds, dark circles and "crossed" squares correspond to $\alpha = \pi/180$, $\pi/36$ and $\pi/18$, respectively. The horizontal dashed curve with a constant value equal 1 corresponds to the matrix phase behavior.

The pronounced dependency of the strains on the direction of the applied field and the lamination angle can be appreciated. For the small lamination angle $\alpha = \pi/180$ and $\theta^{(2)} \cong \pi/4$ the longitudinal strain is 65 times that of the matrix phase. Interestingly, when $\theta^{(2)}$ increases beyond 0.35π a reverse phenomenon is revealed, that is the actuator expands along its thickness and contracts along its longer dimension. Particularly, along the direction where the response of the

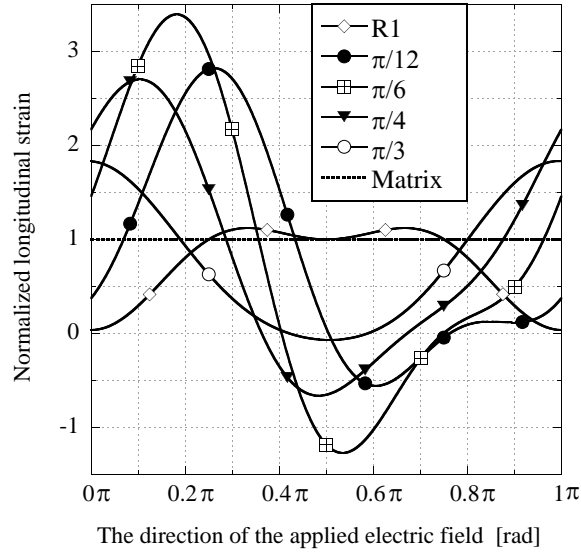


Fig. 3.13: Variations of the normalized longitudinal strains of rank-2 laminated composites with phases whose electrostatic strain responses are identical (the dashed curve), as functions of the direction of the electric field for a few fixed lamination angles. The inclusions' volume fraction is $\lambda^{(i)} = 0.30$.

composite is minimized ($\theta^{(2)} \cong 0.55\pi$) the reversed amplification is of almost 200 times.

Next, we consider the class of composites with phases whose electrostatic strain responses are identical. In Fig. 3.13 the normalized longitudinal strains of a rank-2 laminated composite with phases' moduli contrast $k^{(i)}/k^{(m)} = \mu^{(i)}/\mu^{(m)} = 125$ are shown. The variations are due to changes in the direction of the applied electric field and the lamination angle. The curve marked by clear diamonds corresponds to the rank-1 composite which is obtained by setting $\alpha = 0$. The curves marked by dark circles, “crossed” squares, dark triangles and clear circles correspond to $\alpha = \pi/12, \pi/6, \pi/4$ and $\pi/3$, respectively. The dashed curve corresponds to the behaviors of both the matrix and the inclusion phase.

A significant amplification of the actuation strain is observed in Fig. 3.13. Especially when the lamination angle is $\pi/6$ and $\theta^{(2)} \sim 0.2\pi$ the longitudinal strain is almost 3.5 times the actuation strain of its constituting phases. In the rank-1 composite only slight amplification is predicted (depending on the direction

$k^{(i)}/k^{(m)} = \mu^{(i)}/\mu^{(m)}$	α	$\theta^{(2)}$	$\bar{\varepsilon}_{11}/\varepsilon_{11}^{(m)} = \bar{\varepsilon}_{11}/\varepsilon_{11}^{(i)}$
10	0.22π	0.13π	1.15
100	0.15π	0.19π	3.1
1000	0.06π	0.28π	9
10,000	0.02π	0.31π	26.7
100,000	0.006π	0.33π	83

Tab. 3.1: Optimization of rank-2 composites with $\lambda^{(i)} = 0.30$ and with phases having the same electrostatic strain responses as functions of the contrast between the moduli of the phases.

of the applied electric field), as was notice in Fig. 3.3b.

Motivate by the results of Fig. 3.13, we examine the response of rank-2 composites with different contrasts of the phases' moduli and the same volume fraction as in Eq. (3.66). With the aid of a numerical optimization procedure that was written with the code MATHEMATICA, we obtained the lamination angle and electric field direction that maximize the longitudinal strain for each contrast. The results are summarized in Table 3.1 and Fig. 3.14. Interestingly, we notice the quadratic amplification of the maximal normalized longitudinal strain as the contrast between the phases' moduli increases. An important observation is that we can obtain an amplification of nearly two orders of magnitude of the electromechanical response of the composite.

3.4.2 Composites with fibers with elliptic cross section

Consider the class of composites with fibers with elliptic cross section (see Fig. 3.4) in volume fraction $\lambda^{(i)} = 0.30$, subjected to electrostatic loading conditions. The actuation strains normal to the direction of the applied electric field will vary with the direction of the applied field relative to the principal axes of the elliptic cross section (θ in Fig. 3.4). Thus, for given phases properties and inclusions' aspect ratio γ we can determine the direction along which the response of the composite is maximized. As was noted in Subsection 3.3.2, the elliptic cross section becomes a circle and a layer in the limits $\gamma = 1$ and $\gamma \rightarrow 0$, respectively. For convenience,

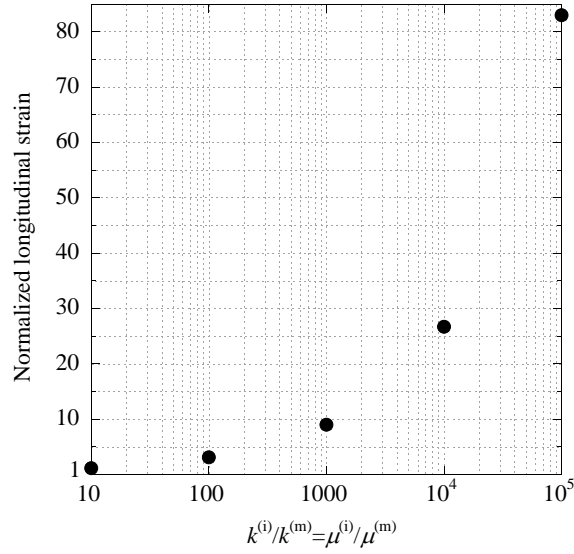


Fig. 3.14: Normalized longitudinal strains of rank-2 composites with $\lambda^{(i)} = 0.30$ along the directions where the electromechanical responses are maximized as functions of the contrast between the moduli of the phases.

in the sequel, these limiting cases will be indicated as TI and R1, respectively.

Similar to the previous Subsection we begin with composites with softer matrices and stiffer conducting inclusions. In Fig. 3.15 shown are the variations of the normalized longitudinal strains of composites with fibers with elliptic cross section as functions of the direction of the applied electric field. The curves marked by clear diamonds, dark circles, “crossed” squares and dark triangles correspond to $\gamma = 0.0005$, $\gamma = 0.001$, $\gamma = 0.25$ and $\gamma = 0.5$, respectively. The curve for the circular cross section is marked by clear circles and the dashed curve shows the response of the homogeneous matrix phase.

We notice that the actuation strains are very sensitive to the direction of the applied electric field. We also note the dependency of the strains on the inclusions’ aspect ratio. Above $\gamma = 0.001$ the amplification of the actuation strain is obtained at $\theta \cong \pi/4$, while as the inclusion shape becomes thinner, the maximum is obtained at higher angles. Specifically, when $\gamma = 0.0005$ and $\theta = \pi/3$ the longitudinal strain is amplified by a factor of 1.5. The advantage of the anisotropic EAPCs is clear when comparing their performances to that of the transversely isotropic composites

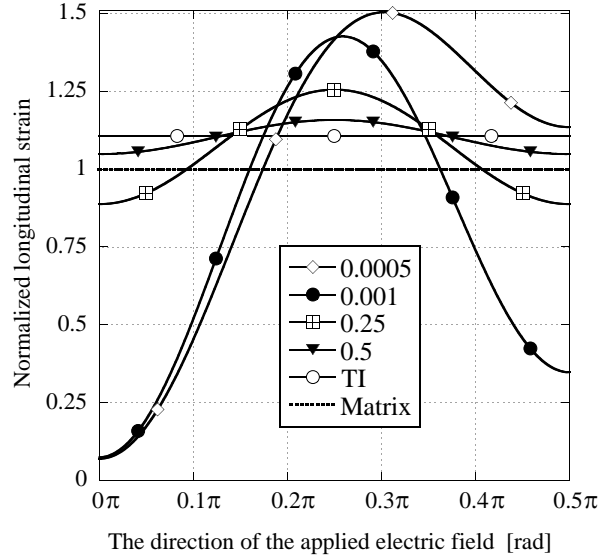


Fig. 3.15: The normalized longitudinal strains of composites with fibers with elliptic cross section with $\lambda^{(i)} = 0.30$ as functions of the direction of the electric field and the inclusions' aspect ratio. The dashed curve shows the response of the homogeneous matrix phase.

with circular fibers.

As in the previous Subsection, we consider a second class of composites with fibers with elliptic cross section in which the phases are having similar electrostatic strain responses. Shown in Fig. 3.16 are results for the normalized longitudinal strains as functions of the applied electric field direction for a few different inclusions' aspect ratio. The contrast between the properties of the phases are $k^{(i)}/k^{(m)} = 10^5$ and $\mu^{(i)}/\mu^{(m)} = 70$ (as in Fig. 3.12). The caption is similar to the one in Fig. 3.15. We notice the non-monotonous dependency of the maximal actuation strain on the aspect ratio of the inclusion. In contrast with the results in Fig. 3.12, maximum of 25% amplification is obtained with an aspect ratio of $\gamma = 0.1$.

The non-monotonous dependency of the strains on the inclusions' aspect ratio is demonstrated in Fig. 3.17. The variations of the normalized longitudinal strains as functions of the inclusions' aspect ratio are shown for fixed electric field direction $\theta = \pi/4$. The curves marked by clear squares, dark circles, "crossed" squares and

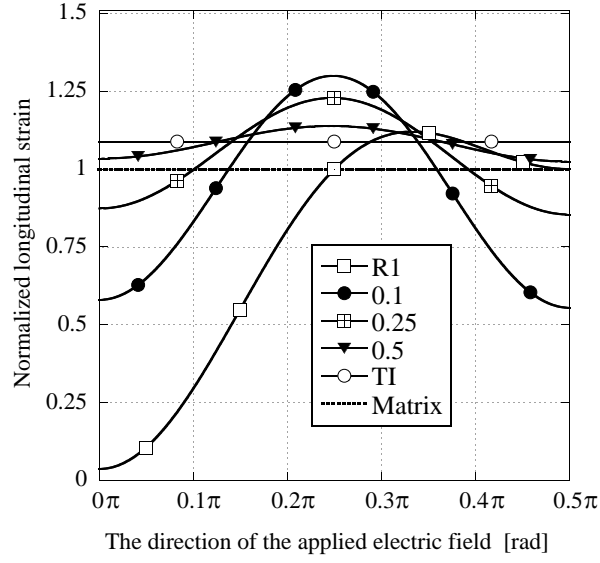


Fig. 3.16: Normalized longitudinal strains of composites with fibers with elliptic cross section where the electrostatic strain responses of the phases are identical. The strains are shown as a function of the direction of the electric field for a few fixed inclusions' aspect ratio. The inclusions' volume fraction is $\lambda^{(i)} = 0.30$.

dark diamonds correspond to phases' contrast $k^{(i)}/k^{(m)} = \mu^{(i)}/\mu^{(m)} = 10, 100, 1000$ and $10,000$, respectively. A composite containing thin stiff and conducting fibers may attain a maximal amplification of 40%.

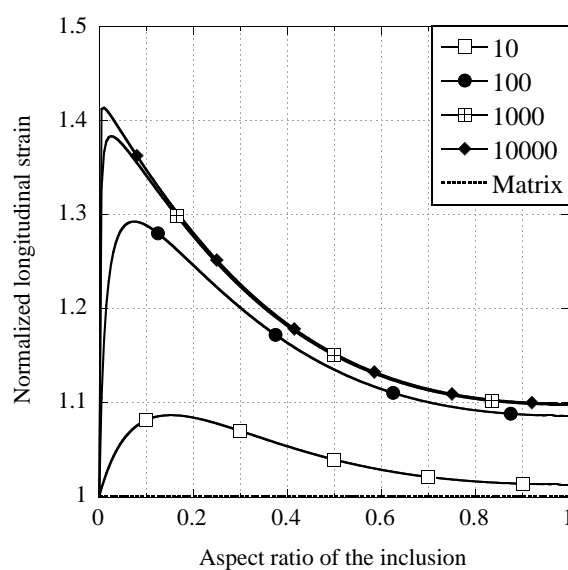


Fig. 3.17: Normalized longitudinal strains of composites with fibers with elliptic cross section with $\lambda^{(i)} = 0.30$ and phases having similar electrostatic strain responses, as functions of the inclusions' aspect ratio. The variations are shown for a few fixed contrast $k^{(i)}/k^{(m)} = \mu^{(i)}/\mu^{(m)} = 10, 100, 1000$ and $10,000$. The dashed curve corresponds to the behavior of the matrix phase.

4. FEM SOLVER FOR EAPCS

The range of possibilities that can be gained by making use of EAPCs was demonstrated in Chapter 3. However, in order to consider more realistic microstructures a more detailed analysis is required. To accomplish this and other specific details there is a need for an appropriate numerical tool that provides a solution for the coupled electromechanical problem. The commercial finite element (FE) code ABAQUS is used to simulate this problem. This FE solver has a well established built-in ability to deal with large deformation problems as well as electrostatics problems. At the present, however, this FE solver doesn't have a solution mode for a coupled electromechanical problem of solids undergoing large deformation. The only available coupled mode is a "piezoelectric" mode in small deformation elasticity. Thus, an external FORTRAN code is written to overcome this limitation.

In the external procedure, initially, the specimen geometry, mesh, the properties of the phases, and the boundary conditions are defined in a manner which is compatible with the required input files for the FE solver. Next ABAQUS in an "electrostatic" mode is used to determine the electric field in the composite by solving the governing equations of electrostatics. The data concerning the electromechanical induced loads (the loads due to Maxwell stress) is determined and prepared in a manner that can be used by ABAQUS in a "mechanical" mode. The deformations resulting in the composite due to these loads are determined at the end of this stage.

A crucial aspect is that this external code is programmed to do both, to generate the electrical induced loads and to interpret the data concerning the geometry of the EAPC in the form provided by the FE solver. This is because the electromechanical loads result in deformation of the EAPC, and there is a need to account

for the evolution of the geometry to determine the variations in the electric fields and the corresponding induced loads. By nature this process is iterative where the required data (geometry and electromechanical loads) is transferred back and forth between the FE solver and the external code. The process need to be repeated until an equilibrium state is achieved.

4.1 *The iterative procedure*

Consider a strip of a heterogeneous hyperelastic dielectric lying between two parallel and flexible electrodes with fixed potentials $\hat{\phi}$, as in Fig. 2.2, subjected to plane-strain boundary conditions. In each iteration, first the electromechanical induced loads due to the Maxwell stress are determined from the electrical simulation. Then by using the `INITIAL CONDITIONS, TYPE=STRESS` parameter in ABAQUS (Hibbitt et al., 2005), these loads are introduced into the model as described below.

When initial stresses are prescribed in ABAQUS, the initial stress state may not be an exact equilibrium state for the finite element model. Therefore, an initial step is executed to allow ABAQUS to check for equilibrium and iterate, if necessary, to achieve equilibrium. The equilibrium is achieved in the following manner:

1. An additional set of artificial stresses is defined at each material point. These stresses are equal in magnitude to the initial stresses but are of opposite sign. The sum of the material point stresses and these artificial stresses results in zero internal forces at the beginning of the step.
2. The internal artificial stresses are ramped off linearly in time during the first solution step. In the deformed state at the end of the step the artificial stresses have been removed completely and the remaining stresses in the material will be in equilibrium.

Thus, according to “ABAQUS pre-stress formulation” at the end of this initial step a deformation from the “equilibrium” state to the reference will result in a

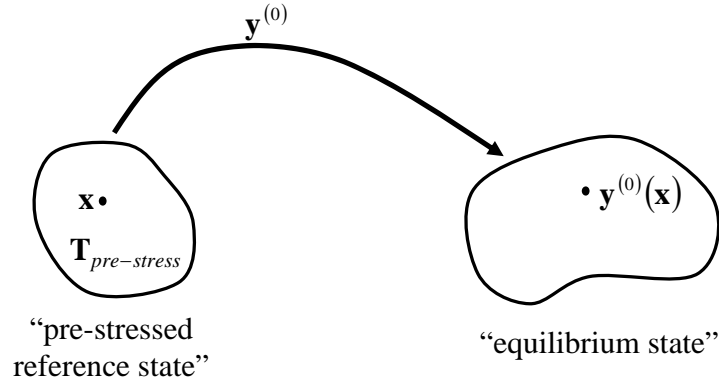


Fig. 4.1: Deformation of a medium with initial stresses.

stress state such that in the reference configuration

$$\mathbf{T} \left(\mathbf{A}^{(0)-1} \right) = \mathbf{T}_{pre-stress}, \quad (4.1)$$

where $\mathbf{A}^{(0)} = \nabla_{\mathbf{x}} \mathbf{y}^{(0)}$, and $\mathbf{T}_{pre-stress}$ is the prescribed initial stress in the “reference” configuration (Fig. 4.1).

In the coupled electromechanical problem, where the actuation strain is due to the Maxwell stress, the stress field in the **deformed** configuration is known (*i.e.*, $\mathbf{T}_{post-stress}$). Therefore, we can not use “ABAQUS pre-stress formulation” to calculate directly the deformation of the dielectric. In fact, to determine a configuration where the sum of the mechanical and the Maxwell stresses is in equilibrium, the tool provided by ABAQUS required us to determine a configuration such that if we will apply $-\mathbf{T}_M$ on that configuration as a pre-stress, the “equilibrium” state will be our reference configuration. To accomplish this task we follow the procedure shown in Fig. 4.2.

In some approximate way by applying a pre-stress $+\mathbf{T}_M$ at the reference state, the configuration $\mathbf{y}_{g(1)}$ in Fig. 4.2 provides a first iteration for the deformed “loaded” configuration. Then, in accordance with “ABAQUS pre-stress formulation” an approximation for the **reference** configuration $\mathbf{x}_{g(1)}$ is determined by applying $-\mathbf{T}_M$ at this configuration such that

$$\mathbf{T} \left(\mathbf{F}_{g(1)}^{-1} \right) + \mathbf{T}_M = 0. \quad (4.2)$$

We assume that $\mathbf{u}_{g(1)} = \mathbf{y}_{g(1)} - \mathbf{x}_{g(1)}$ represent the displacement from the reference configuration to the deformed configuration and make a second guess for the deformed configuration in the form

$$\mathbf{y}_{g(2)} = \mathbf{x}_0 + \mathbf{u}_{g(1)} = \mathbf{y}_{g(1)} + (\mathbf{x}_0 - \mathbf{x}_{g(1)}). \quad (4.3)$$

Note that

$$\begin{aligned} \mathbf{A}_{g(2)} &= \frac{\partial \mathbf{y}_{g(2)}}{\partial \mathbf{x}_0} \\ &= \mathbf{I} + \mathbf{A}_{g(1)} - \mathbf{A}_{0(1)} \\ &= \mathbf{I} + (\mathbf{I} - \mathbf{F}_{g(1)})\mathbf{A}_{g(1)}. \end{aligned} \quad (4.4)$$

Assuming that $\mathbf{y}_{g(2)}$ is a better approximation for the actual deformed configuration, we apply the pre-stress $-\mathbf{T}_M$ on this configuration to obtain a new (hopefully better) “undeformed” configuration $\mathbf{x}_{g(2)}$. In the next iteration we compute the displacement $\mathbf{u}_{g(2)} = \mathbf{y}_{g(2)} - \mathbf{x}_{g(2)}$ and then $\mathbf{y}_{g(3)} = \mathbf{x}_0 + \mathbf{u}_{g(2)}$ as an improved estimate for the current configuration and then apply $-\mathbf{T}_M$ to determine $\mathbf{x}_{g(3)}$. This procedure can be repeated until a convergence criterion in the form $\mathbf{x}_0 - \mathbf{x}_{g(i)}$ smaller than some threshold is attained. Notice that we do not have a rigorous proof that this scheme will converge.

In the iterative procedure presented in Fig. 4.3 the above described scheme is extended to account for the changes in the Maxwell stress due to the deformation of the medium. To verify the accuracy and capability of this procedure, we consider first a homogeneous sample made out of incompressible neo-Hookean dielectric and compare the FE simulation with the analytic solution (see Appendix B). The convergence of the numerical results with increasing the number of elements was examined too.

4.2 Plane-strain simulation

When the specimen is subjected to plane-strain loading conditions, we have to take into account the out-of-plane stress component. Suppose that each single phase is an incompressible neo-Hookean dielectric material with energy-density function as

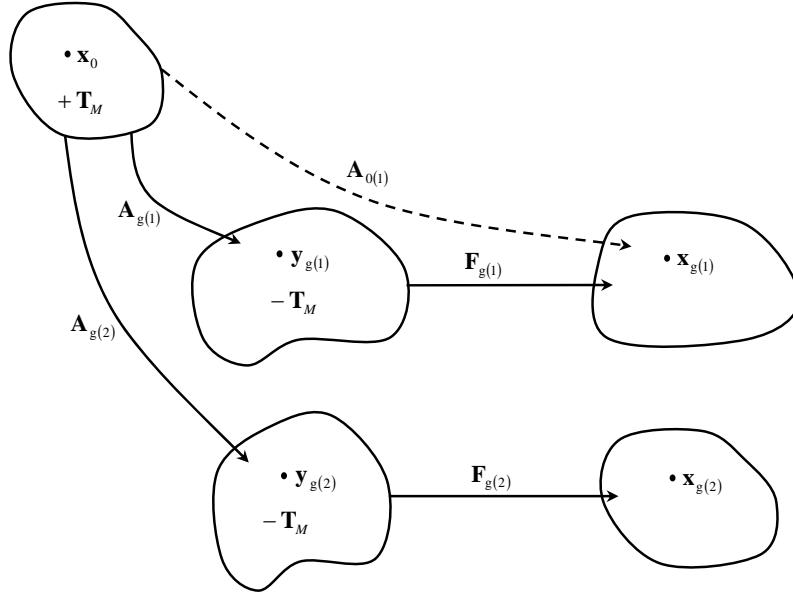


Fig. 4.2: Schematic iterative procedure of a medium with “post-stresses”.

in expression (3.7). Thus, we set in the expression for the Cauchy stress

$$\mathbf{T}^{(r)} = \mu^{(r)} \mathbf{A} \mathbf{A}^T - p^{(r)} \mathbf{I} + t^{(r)} \mathbf{I}_3, \quad (4.5)$$

where

$$\mathbf{I}_3 = \begin{pmatrix} 0 & 0 & 0 \\ 0 & 0 & 0 \\ 0 & 0 & 1 \end{pmatrix},$$

and

$$t^{(r)} = \epsilon_0 k^{(r)} (A_{11} E_1 + A_{21} E_2)^2 + \mu^{(r)} (A_{22}^2 + A_{12}^2 - 1),$$

and apply the initial stress field

$$\mathbf{T}_{pre-stress}^{(r)} = -\mathbf{T}_M^{(r)} - t^{(r)} \mathbf{I}_3, \quad (4.6)$$

instead of $-\mathbf{T}_M^{(r)}$.

4.3 Application to hexagonal unit cell

In this Section we applied the iterative numerical procedure to simulate the overall actuation of a two-dimensional hexagonal unit cell made out of two incompress-

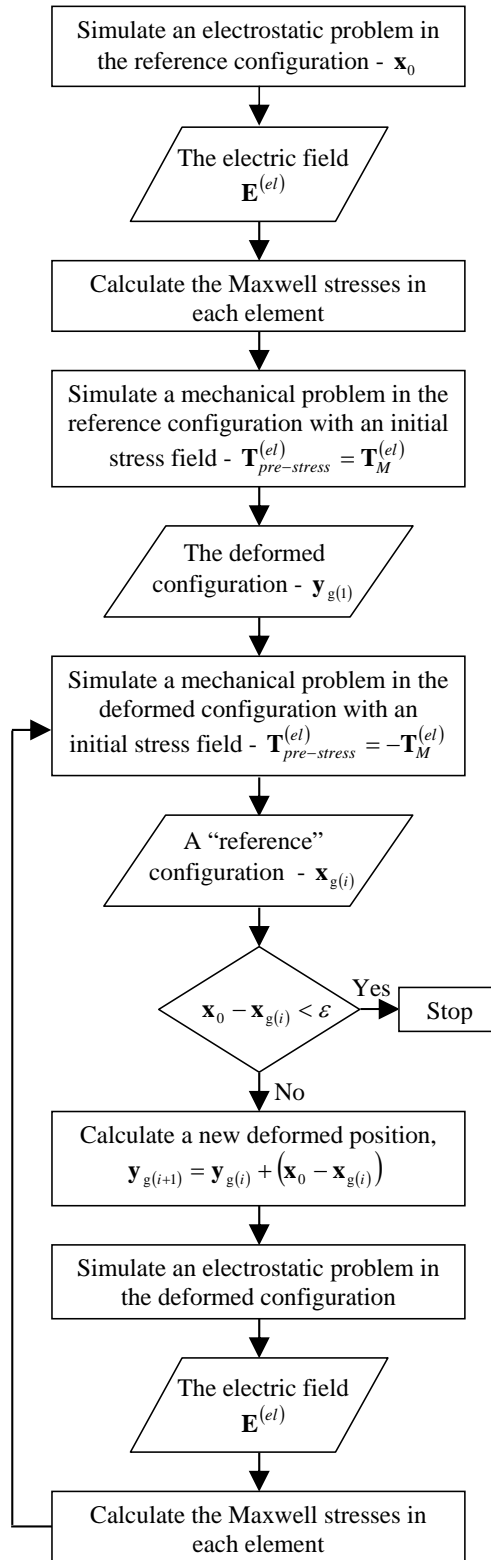


Fig. 4.3: Schematic representation of the steps followed by the iterative procedure

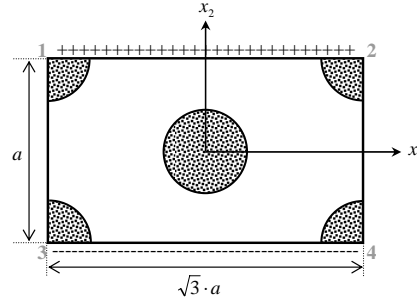


Fig. 4.4: Hexagonal unit cell

ible neo-Hookean dielectric phases with energy-density function (3.7), subjected to plane-strain loading conditions.

The response of the composite is determined by application of appropriate homogeneous electric boundary conditions on the top and the bottom faces of the unit cell (Fig. 4.4). Following the works of Aravas et al. (1995), deBotton and Tevet-Deree (2004) and deBotton et al. (2006), in the reference configuration the two-phase hexagonal unit cell is a cuboid whose rear and front faces are the ones normal to the fibers direction and the ratio between the lengths of the two transverse faces is $\sqrt{3}$ (see Fig. 4.4). For convenience we choose a coordinate system whose axes are normal to the faces of the unit cell with x_3 along the fibers, and x_1 aligned with the longer face.

A built in compressible neo-Hookean constitutive law was used to define the strain energy-density functions of the matrix and the fiber phases in the mechanical problem. To impose incompressibility in both phases the bulk modulus was chosen to be two orders of magnitude larger than the shear modulus of the stiffer phase.

To enforce the periodic displacement boundary conditions on the in-plane faces, we used a symmetry condition on the left and bottom faces, and on the right and top faces the "linear multi-point constrain equation" procedure available in ABAQUS. This procedure allows us to impose a linear combination of nodal variables in the form

$$\alpha_1 u_{i_1}^{n_1} + \alpha_2 u_{i_2}^{n_2} + \dots + \alpha_N u_{i_N}^{n_N} = 0, \quad (4.7)$$

where $u_{i_S}^{n_S}$ ($S = 1, 2, \dots, N$) is the nodal variable at node n_S , degree of freedom i_S ,

and α_S are the coefficients defining the relative motion of the nodes. The data lines of the "EQUATION" procedure are provided in the form:

*EQUATION

N (the number of terms in the equation)

n_1, i_1, α_1 (the node number, degree of freedom, coefficient)

n_2, i_2, α_2

⋮

n_N, i_N, α_N .

According to the periodicity conditions, the right face and the top face remain straight and parallel to the left face and the bottom face, respectively. Thus, for example, to impose the constraints in node number 2 and nodes number 1 and 4 in Fig. 4.4, we enter the following commands:

*EQUATION

2

2, 2, 1.

1, 2, -1.

*EQUATION

2

2, 1, 1.

4, 1, -1.

4.4 Naive estimate

To the best knowledge of the author, there are no analytical solutions or estimates for the coupled electromechanical response of fiber composites in the limit of finite deformations elasticity. For the corresponding purely mechanical case, the response of transversely isotropic fiber composites made out of two incompressible neo-Hookean phases undergoing finite deformations was considered by deBotton et al. (2006). Moreover, Hashin (1970) solved the corresponding purely electrical

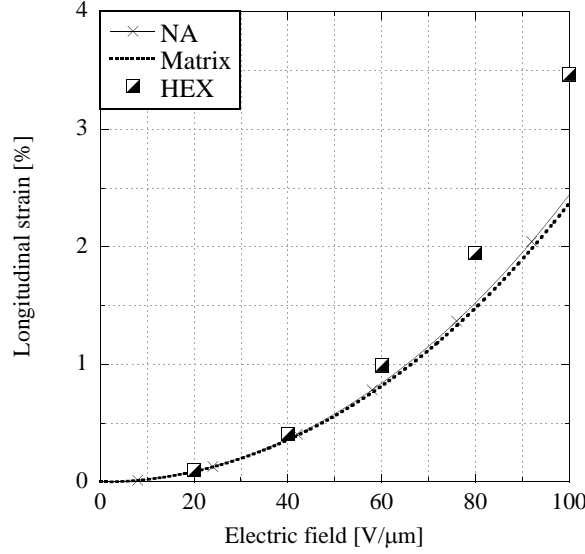


Fig. 4.5: Longitudinal strain of periodic composite with hexagonal unit cell and with $\lambda^{(i)} = 0.45$ and a corresponding naive estimate, as functions of the excitation electric field. The dashed curve corresponds to the behavior of the matrix phase.

problem. Combining these two separated solutions, we can determine a “naive” estimate for the actuation strain of hyperelastic transversely isotropic dielectrics under plane-strain loading conditions. In this estimate we assume that the composite is a homogeneous material with effective in-plane properties like in deBotton et al. (2006) and Hashin (1970), respectively.

The macroscopic deformation gradient $\bar{A}_{11}^{(\text{NA})}$, due to the excitation field $\bar{\mathbf{E}}^0 = E_0 \hat{\mathbf{x}}_2$, then can be obtained similarly to Eq. (B-7) by replacing the shear and the dielectric moduli with $\tilde{\mu}_T^{(\text{TI})}$ and $\tilde{k}_T^{(\text{TI})}$, respectively, *i.e.*,

$$\bar{A}_{11}^{(\text{NA})} = \left[1 - \frac{\epsilon_0 \tilde{k}_T^{(\text{TI})}}{\tilde{\mu}_T^{(\text{TI})}} (E_0)^2 \right]^{-\frac{1}{4}}. \quad (4.8)$$

4.5 Examples

The application of the iterative procedure to simulate the actuation strain of fiber composites with hexagonal unit cell is demonstrated in this Section. In the following examples, as in Chapter 3, we examine the longitudinal Eulerian strain

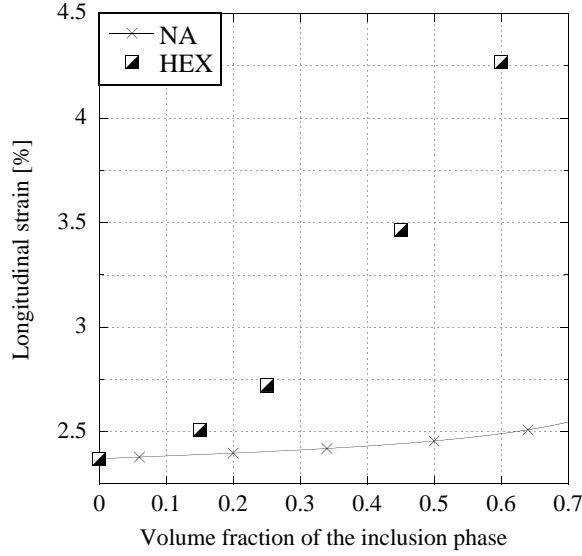


Fig. 4.6: FEM simulations of periodic composites and naive estimates with $\lambda^{(i)} = 0.15, 0.25, 0.45$ and 0.60 as functions of the volume fraction of the inclusions.

response (\bar{E}_{11}) of a sample (see Fig. 4.4) in its longer dimension due to the applied electric field along its thickness (\bar{E}_2). We consider composites made out of two incompressible neo-Hookean dielectric phases with inclusions' volume fractions $\lambda^{(i)} = 0.15, 0.25, 0.45$ and 0.60 . The two phases are characterized by elastic shear moduli $\mu^{(i)}$ and $\mu^{(m)}$, and dielectric constants $k^{(i)}$ and $k^{(m)}$.

Shown in Fig. 4.5 are the variations of the longitudinal strain of a periodic composite with hexagonal unit cell (black and white squares) and the naive estimate for transversely isotropic composite (cross marks) as functions of the excitation electric field. The volume fraction of the inclusions phase is $\lambda^{(i)} = 0.45$ and the phases properties are similar to those in the work of Huang et al. (2004). Specifically, the properties of the flexible matrix are $\mu^{(m)} = 10[\text{MPa}]$ and $k^{(m)} = 10$, and those of the conductive inclusions phase are $\mu^{(i)} = 80[\text{MPa}]$ and $k^{(i)} > 10^5$. For comparison, also shown is the response of the homogeneous matrix phase to the applied excitation field (dashed curve).

We note that the naive approach underestimates the simulations results. In agreement with the experimental findings of Huang et al. (2004), we too find that the electromechanical response of the flexible matrix can be enhanced when

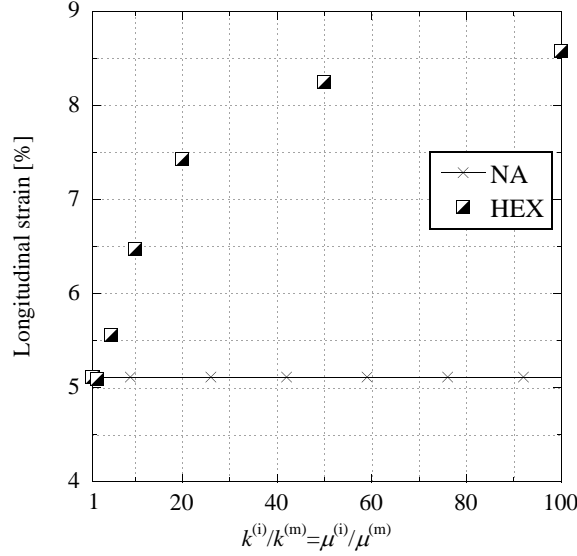


Fig. 4.7: FEM simulations and naive estimates of composite whose phases have identical strain responses, and with $\lambda^{(i)} = 0.45$ for the longitudinal strain as functions of the phases' contrast.

combining it with high-dielectric conductive inclusions. We observe that the strain response of the periodic composite with $\lambda^{(i)} = 0.45$ is 45% higher than the matrix response when $\bar{E}_2 = 100[\text{V}/\mu\text{m}]$.

The longitudinal strains of periodic composites with $\lambda^{(i)} = 0.15, 0.25, 0.45$ and 0.60 due to excitation electric field $\bar{E}_2 = 100[\text{V}/\mu\text{m}]$ are shown in Fig. 4.6. The properties of the inclusion and the matrix phases are same as in Fig. 4.5. We note that as the conductive inclusions' volume fraction increases the strain response of the composite is increasing too. When $\lambda^{(i)} = 0.6$ we observe that the response of the periodic composite is 80% higher than that of the matrix.

As in Sections 3.1.2 and 3.3.6, we consider the case of periodic composites with phases having similar electrostatic strain response. The inclusion's volume fraction is $\lambda^{(i)} = 0.45$. Results, in terms of the longitudinal strains as functions of the phases' contrast, are shown in Fig. 4.7 for a fixed activation field $\bar{E}_2 = 50[\text{V}/\mu\text{m}]$. The horizontal line represents the naive estimate which, in this case, coincides with the response of the two phases. When the ratio of the phases' moduli increases above 2.5 an *amplification* of the strain response is obtained. In particular, with

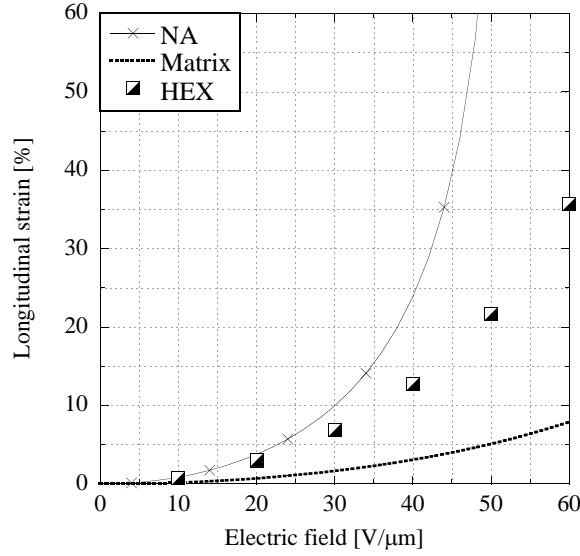


Fig. 4.8: FEM simulations of periodic composite and naive estimate for composites with $\lambda^{(i)} = 0.45$ as functions of the excitation electric field.

$k^{(i)}/k^{(m)} = 100$ the composite' longitudinal strain is 1.7 times the longitudinal strain of its constituting phases.

To demonstrate the capability of the numerical procedure in the limit of large actuation strains, we consider next a case of a periodic composite with $\lambda^{(i)} = 0.45$ made out of soft high-dielectric inclusions in a stiff polymeric matrix, such that $\mu^{(m)}/\mu^{(i)} = 100$ and $k^{(i)}/k^{(m)} = 5$. The variations of the longitudinal strain as functions of the excitation electric field are shown in Fig. 4.8. We note that when the applied field is about $60[\text{V}/\mu\text{m}]$, an elongation of 35% is obtained.

5. CONCLUDING REMARKS

A continuum-mechanics framework for investigating the mechanical response of heterogeneous media undergoing *finite* deformations due to nonlinear electrostatic excitation was developed. The governing equations for the coupled electromechanical problem, the set of boundary conditions at the boundary of the composite, and the appropriate jump conditions at the interfaces are derived. These were applied to the class of rank-1 laminated composites to obtain explicit expression for the macroscopic actuation strains.

In the limit of infinitesimal deformation theory of elasticity we followed the work of Levin (1967), in the context of thermomechanical coupling, and introduced a systematic method for representing and determining the macroscopic Maxwell stress in heterogeneous materials. This is expressed in terms of a fourth-order electromechanical coupling tensor depending on the concentration tensors relating the average electric and strain fields with their corresponding counterparts in the individual phases. The advantage of this presentation results from the fact that a large number of exact expressions and estimates for the concentration tensors can be extracted from well-known solutions and estimates for the uncoupled electrostatic and mechanical problems. The method was applied to derive an exact expression for the response of sequentially laminated composites. Additionally, estimates for the overall behavior of composites were obtained on the basis of the HS bounds of Willis (1977), and third-order bounds on the effective dielectric and elastic moduli (*e.g.*, Torquato, 1991; Gibiansky and Torquato, 1995).

We further developed a numerical tool to provide a solution for the electromechanical response of heterogeneous hyperelastic dielectrics. The numerical calculations are based on finite element simulations by application of iterative procedure in the commercial code ABAQUS. Applying the iterative procedure, we

carried out simulations of the actuation strains of fiber composites with periodic hexagonal unit cell.

Results for the electromechanical coupling in transversely isotropic rank-6 laminated composites and periodic composites with hexagonal unit cell were compared with corresponding HS and third-order estimates. It was found that in most cases the HS and the higher order estimates can be used to approximate the electromechanical coupling in the periodic composite. In all cases the coupling in the rank-6 laminate was the weakest. The pronounced dependency of the electromechanical coupling on the composites' microstructure was demonstrated by considering a class of two-phase composites in which the electrostatic strain response of the two phases is identical. We demonstrated that an improvement in the overall actuation strain can be achieved with appropriate spatial arrangement of the phases. In particular, we have shown that the overall response of a composite actuator can be better than the responses of its constituents.

Finally, we considered the class of anisotropic EAPCs, including rank-2 laminated composites and composites with fibers with elliptic cross section, and determined the best arrangement for maximal actuation under given boundary conditions. We found that the electromechanical coupling response of a soft dielectric matrix can be enhanced more than 65 times by adding 30% particles of conductive oligomer. We note that these findings are in agreement with recent experimental results (Zhang et al., 2002; Huang et al., 2004). We further demonstrated that severe amplification of the actuation strain is attained as the contrast between the moduli of the phases increases.

APPENDIX

A. WALPOLE'S NOTATION

In Section 3.3.2 we followed the notation of Walpole (1969) (see also Walpole, 1981) to express the HS estimates for the macroscopic Maxwell stress. In this appendix we summarize this notation. Consider a transversely isotropic material whose isotropy plane is perpendicular to a unit vector \mathbf{n} , and the two elementary second-order tensors

$$a_{ij} = n_i n_j \quad \text{and} \quad b_{ij} = \delta_{ij} - n_i n_j,$$

such that $\delta_{ij} = a_{ij} + b_{ij}$, $a_{ik} a_{kj} = a_{ij}$, $b_{ik} b_{kj} = b_{ij}$, and $a_{ik} b_{kj} = a_{jk} b_{ki} = 0$. The most general second-order tensor admitting transverse isotropy is

$$\mathbf{c}_{ij} = k_L a_{ij} + k_T b_{ij}, \tag{A-1}$$

where k_L and k_T are arbitrary coefficients. We express this second-order tensor in the form

$$\mathbf{c} = (k_L, k_T). \tag{A-2}$$

If $\mathbf{c}' = (k'_L, k'_T)$ is a second transversely isotropic tensor, the inner product between the two tensors is

$$\mathbf{c}\mathbf{c}' = (k_L k'_L, k_T k'_T). \tag{A-3}$$

Particularly, if $k'_L = 1/k_L$ and $k'_T = 1/k_T$ then \mathbf{c}' is the inverse of \mathbf{c} , and we note that in this notation the identity second-order tensor is

$$\mathbf{I} = (1, 1). \tag{A-4}$$

The set of elementary fourth-order tensors is (Walpole, 1981),

$$\begin{aligned}
E_{ijkl}^{(1)} &= \frac{1}{2}b_{ij}b_{kl}, \\
E_{ijkl}^{(2)} &= a_{ij}a_{kl}, \\
E_{ijkl}^{(3)} &= \frac{1}{2}(b_{ik}b_{jl} + b_{jk}b_{il} - b_{ij}b_{kl}), \\
E_{ijkl}^{(4)} &= \frac{1}{2}(b_{ik}a_{jl} + b_{il}a_{jk} + b_{jl}a_{ik} + b_{jk}a_{il}), \\
E_{ijkl}^{(5)} &= a_{ij}b_{kl}, \\
E_{ijkl}^{(6)} &= b_{ij}a_{kl}.
\end{aligned} \tag{A-5}$$

The inner products between these tensors are summarized in the following table.

	$\mathbf{E}^{(1)}$	$\mathbf{E}^{(2)}$	$\mathbf{E}^{(3)}$	$\mathbf{E}^{(4)}$	$\mathbf{E}^{(5)}$	$\mathbf{E}^{(6)}$
$\mathbf{E}^{(1)}$	$\mathbf{E}^{(1)}$	0	0	0	0	$\mathbf{E}^{(6)}$
$\mathbf{E}^{(2)}$	0	$\mathbf{E}^{(2)}$	0	0	$\mathbf{E}^{(5)}$	0
$\mathbf{E}^{(3)}$	0	0	$\mathbf{E}^{(3)}$	0	0	0
$\mathbf{E}^{(4)}$	0	0	0	$\mathbf{E}^{(4)}$	0	0
$\mathbf{E}^{(5)}$	$\mathbf{E}^{(5)}$	0	0	0	0	$2\mathbf{E}^{(2)}$
$\mathbf{E}^{(6)}$	0	$\mathbf{E}^{(6)}$	0	0	$2\mathbf{E}^{(1)}$	0

A general fourth-order transversely isotropic tensor is a linear combination of these six elementary tensors, *i.e.*,

$$\mathbf{M} = 2\kappa_T \mathbf{E}^{(1)} + n \mathbf{E}^{(2)} + 2\mu_T \mathbf{E}^{(3)} + 2\mu_L \mathbf{E}^{(4)} + l \mathbf{E}^{(5)} + l \mathbf{E}^{(6)}. \tag{A-6}$$

The fourth-order ‘‘unit’’ tensor is $\mathfrak{J} = \mathbf{E}^{(1)} + \mathbf{E}^{(2)} + \mathbf{E}^{(3)} + \mathbf{E}^{(4)}$.

Following Walpole (1981) the fourth-order tensor \mathbf{M} may be written in the form

$$\mathbf{M} = (2\kappa_T, l, l, n, 2\mu_T, 2\mu_L), \tag{A-7}$$

and the corresponding fourth-order ‘‘unit’’ tensor is

$$\mathfrak{J} = (1, 0, 0, 1, 1, 1), \tag{A-8}$$

If \mathbf{M}' is another fourth-order tensor defined by attaching a prime to each of the coefficients in Eq. (A-7), the inner product $\mathbf{M}\mathbf{M}'$ is

$$\mathbf{M}\mathbf{M}' = (4\kappa_T \kappa_T' + 2ll', 2\kappa_T' l + l'n, 2\kappa_T l' + ln', 2ll' + nn', 4\mu_T \mu_T', 4\mu_L \mu_L'). \tag{A-9}$$

The inverse of \mathbf{M} is

$$\mathbf{M}^{-1} = (n/2\Delta, -l/2\Delta, -l/2\Delta, \kappa_T/\Delta, 1/2\mu_T, 1/2\mu_L), \quad (\text{A-10})$$

where $\Delta = \kappa_T n - l^2$. The inner product between a fourth-order and a second-order tensors $M_{ijkl}c_{kl}$ results in a second-order tensor

$$\mathbf{M} : \mathbf{c} = (nk_L + 2lk_T, lk_L + 2\kappa_T k_T). \quad (\text{A-11})$$

The fourth-order tensor resulting from an outer product between two second-order tensors (*i.e.*, $M_{ijkl} = c_{ik}c'_{jl}$) is

$$\mathbf{c} \otimes \mathbf{c}' = (k_T k'_T, 0, 0, k_L k'_L, k_T k'_T, \frac{1}{2}(k_L k'_T + k'_L k_T)). \quad (\text{A-12})$$

B. ANALYTIC SOLUTION FOR A HOMOGENEOUS BODY

In Section 4.4 we used the analytic expression for the electromechanical strain response of a *homogeneous* incompressible neo-Hookean dielectric to obtain a “naive” estimate. Here we outline the solution of this problem.

Consider a homogeneous incompressible neo-Hookean dielectric with energy-density function Eq. (3.7) subjected to boundary loading conditions as depicted in Fig. 2.2. The electric field in the reference configuration due to the potential differences ϕ is

$$\mathbf{E}^0 = -\nabla_{\mathbf{x}}\phi = E_0\hat{\mathbf{x}}_2. \quad (\text{B-1})$$

The electric displacement field in the current configuration is obtained by Eq. (3.10) together with the relation

$$\mathbf{E} = \mathbf{A}^{-T}\mathbf{E}^0. \quad (\text{B-2})$$

Then we can determine the Maxwell stress tensor via Eq. (3.11), that is

$$\mathbf{T}_M = \mathbf{B} : (\mathbf{A}^{-T}\mathbf{E}^0) \otimes (\mathbf{A}^{-T}\mathbf{E}^0). \quad (\text{B-3})$$

Considering the mechanical boundary condition (2.48) specialized to the case $\mathbf{t} = \mathbf{0}$ and neglecting the fringing field effect (*i.e.*, $\mathbf{T}_M^{(0)} = \mathbf{0}$) we have

$$\mathbf{T}\hat{\mathbf{n}} = -\mathbf{T}_M\hat{\mathbf{n}}. \quad (\text{B-4})$$

We note that these boundary conditions are homogeneous, and since the body is homogeneous,

$$\mathbf{T} = -\mathbf{T}_M. \quad (\text{B-5})$$

Now, by using expression (3.14) for the Cauchy stress tensor together with

expression (B-3) in Eq. (B-5) we obtain an equation for the deformation gradient

$$\begin{aligned} & \mu \begin{pmatrix} A_{11}^2 + A_{12}^2 & A_{12}/A_{11} \\ A_{12}/A_{11} & 1/A_{11}^2 \end{pmatrix} - p \begin{pmatrix} 1 & 0 \\ 0 & 1 \end{pmatrix} \\ &= -\epsilon_0 k \begin{pmatrix} 0 & 0 \\ 0 & (A_{11}E_0)^2 \end{pmatrix} + \frac{\epsilon_0}{2} \begin{pmatrix} (A_{11}E_0)^2 & 0 \\ 0 & (A_{11}E_0)^2 \end{pmatrix}, \end{aligned} \quad (\text{B-6})$$

where we assumed $A_{21} = 0$ and due to the incompressibility $A_{22} = 1/A_{11}$. Solving this equation we get

$$\begin{aligned} A_{12} &= 0, \\ A_{11} &= \left[1 - \frac{\epsilon_0 k}{\mu} (E_0)^2 \right]^{-\frac{1}{4}}. \end{aligned} \quad (\text{B-7})$$

Finally, we can determine the Eulerian strain tensor

$$\frac{1}{2} (\mathbf{A}^T \mathbf{A} - \mathbf{I}), \quad (\text{B-8})$$

describing the transverse expansion and the normal contraction of the actuator (*i.e.*, E_{11} and E_{22} , respectively).

BIBLIOGRAPHY

- Aravas, N., Cheng, C. and Ponte Castañeda, P. (1995). Steady-state creep of fiber-reinforced composites: Constitutive equations and computational issues, *Int. J. Solids Structures* **32**(15): 2219–2244.
- Bar-Cohen, Y. (2001). EAP history, current status, and infrastructure, in Y. Bar-Cohen (ed.), *Electroactive Polymer (EAP) Actuators as Artificial Muscles*, SPIE press, Bellingham, WA, chapter 1, pp. 3–44.
- Bar-Cohen, Y. (2002). Electroactive polymers as artificial muscles, *J. of Spacecraft and Rockets* **39**: 822–827.
- Benveniste, Y. (1993). Universal relations in piezoelectric composites with eigenstress and polarization-fields 1. binary media - local-fields and effective behavior, *J. Appl. Mech., Trans. ASME* **60**: 265–269.
- Beran, M. J. (1965). Use of the variational approach to determine bounds for the effective permittivity in random media, *Nuovo Cimento* **38**(2): 771–782.
- Berryman, J. G. (2006). Measures of microstructure to improve estimates and bounds on elastic constants and transport coefficients in heterogeneous media, *Mechanics of Materials* **38**(8-10): 732–747.
- Bhattacharya, K., Li, J. Y. and Xiao, Y. (2001). Electromechanical models for optimal design and effective behavior of electroactive polymers, in Y. Bar-Cohen (ed.), *Electroactive Polymer (EAP) Actuators as Artificial Muscles*, SPIE press, chapter 12, pp. 309–330.
- Bustamante, R., Dorfmann, A. and Ogden, R. W. (2008). Nonlinear electroelastostatic: a variational framework, *Zeitschrift für Angewandte Mathematik und Physik* pp. 1–24.
- Coleman, B. D. and Noll, W. (1963). The thermodynamics of elastic material with heat conduction and viscosity, *Arch. Rational. Mech. Anal.* **13**: 167–178.
- deBotton, G. (2005). Transversely isotropic sequentially laminated composites in finite elasticity, *J. Mech. Phys. Solids* **53**(6): 1334–1361.
- deBotton, G. and Hariton, I. (2002). High-rank nonlinear sequentially laminated composites and their possible tendency towards isotropic behavior, *J. Mech. Phys. Solids* **50**(12): 2577–2595.

-
- deBotton, G. and Tevet-Deree, L. (2004). The response of a fiber-reinforced composite with a viscous matrix phase, *J. Composite Materials* **38**(14): 1255–1277.
- deBotton, G., Hariton, I. and Socolsky, E. A. (2006). Neo-Hookean fiber-reinforced composites in finite elasticity, *J. Mech. Phys. Solids* **54**(3): 533–559.
- deBotton, G., Tevet-Deree, L. and Socolsky, E. A. (2007). Electroactive heterogeneous polymers: analysis and applications to laminated composites, *Mechanics of Advanced Materials and Structures* **14**(1): 13–22.
- Dorfmann, A. and Ogden, R. W. (2005). Nonlinear electroelasticity, *Acta. Mech.* **174**(3-4): 167–183.
- Duan, H. L., Karihaloo, B. L., Wang, J. and Yi, X. (2006). Effective conductivities of heterogeneous media containing multiple inclusions with various spatial distributions, *Phys. Rev. B* **73**(174203): 1–13.
- Eringen, A. C. (1963). On the foundations of electroelastostatics, *Int. J. Engng. Sci.* **1**: 127–153.
- Eshelby, J. D. (1957). The determination of the elastic field of an ellipsoidal inclusion, and related problems, *Proc. R. Soc. Lond. A* **241**(1226): 376–396.
- Francfort, G. and Murat, F. (1986). Homogenization and optimal bounds in linear elasticity, *Arch. Rational. Mech. Anal.* **94**(4): 307–334.
- Gei, M. and Magnarelli, L. (2006). The role of multifield theories in the modelling of active materials, in Y. Bar-Cohen (ed.), *Smart Structures and Materials 2006: Electroactive Polymer Actuators and Devices*, Vol. 6168 of *Proc. of SPIE*, San Diego, CA.
- Gibiansky, L. V. and Torquato, S. (1995). Geometrical-parameter bounds on the effective moduli of composites, *J. Mech. Phys. Solids* **43**(1702): 1587–1613.
- Hariton, I. and deBotton, G. (2003). The nearly isotropic behavior of high-rank nonlinear sequentially laminated composites, *Proc. R. Soc. Lond. A* **459**(2029): 157–174.
- Hashin, Z. (1965). On elastic behaviour of fibre reinforced materials of arbitrary transverse phase geometry, *J. Mech. Phys. Solids* **13**(3): 119–134.
- Hashin, Z. (1970). Theory of composite materials, in F. W. Wendt, H. Liebowitz and N. Perrone (eds), *Conf. Mechanics of Composite Materials*, Pergamon Press, New York, pp. 201–242.
- Hashin, Z. and Rosen, B. W. (1964). The elastic moduli of fiber-reinforced materials, *J. Appl. Mech., Trans. ASME* **31**(3): 223–232.

-
- Hashin, Z. and Shtrikman, S. (1962). On some variational principles in anisotropic and nonhomogeneous elasticity, *J. Mech. Phys. Solids* **10**(4): 335–342.
- Hibbitt, D., Karlsson, B. and Sorensen, P. (2005). *ABAQUS/Standard User's Manual, Version 6.5*, ABAQUS ltd., Providence, RI.
- Hill, R. (1963). Elastic properties of reinforced solids: Some theoretical principles, *J. Mech. Phys. Solids* **11**(5): 357–372.
- Hill, R. (1964). Theory of mechanical properties of fiber-strengthened materials: I. elastic behaviour, *J. Mech. Phys. Solids* **12**(4): 199–212.
- Hill, R. (1972). On constitutive macro-variables for heterogeneous solids at finite strain, *Proc. R. Soc. Lond. A* **326**: 131–147.
- Hill, R. and Rice, J. R. (1973). Elastic potentials and the structure of inelastic constitutive laws, *SIAM J. Appl. Math.* **25**: 448–461.
- Huang, C., Zhang, Q. M., deBotton, G. and Bhattacharya, K. (2004). All-organic dielectric-percolative three-component composite materials with high electromechanical response, *Applied Physics Letters* **84**(22): 4391–4393.
- Kankanala, S. V. and Triantafyllidis, N. (2004). On finitely strained magnetorheological elastomers, *J. Mech. Phys. Solids* **52**(12): 2869–2908.
- Landis, C. M. (2004). Non-linear constitutive modeling of ferroelectrics, *Current Opinion in Solid State and Materials Science* **8**(1): 59–69.
- Levin, V. M. (1967). Thermal expansion coefficients of heterogeneous materials, *Mekhanika Tverdogo Tela* **2**(1): 88–94. English translation - *Mechanics of solids*, **2**(1):58-61.
- Li, J. Y. and Rao, N. (2004). Micromechanics of ferroelectric polymer-based electrostrictive composites, *J. Mech. Phys. Solids* **52**(3): 591–615.
- Li, J. Y., Huang, C. and Zhang, Q. M. (2004). Enhanced electromechanical properties in all-polymer percolative composites, *Applied Physics Letters* **84**(16): 3124–3126.
- McMeeking, R. M. and Landis, C. M. (2005). Electrostatic forces and stored energy for deformable dielectric materials, *J. Appl. Mech., Trans. ASME* **72**(4): 581–590.
- Milton, G. W. (1981). Bounds on the electromagnetic, elastic, and other properties of two-component composites, *Phys. Rev. Lett.* **46**(8): 542–545.
- Milton, G. W. (1982). Bounds on the elastic and transport properties of two-component composites, *J. Mech. Phys. Solids* **30**(3): 177–191.

-
- Milton, G. W. (1986). Modeling the properties of composites by laminates, in J. Ericksen, R. Kinderlehrer, R. Kohn and J. L. Lions (eds), *Homogenization and Effective Moduli of Materials and Media*, Springer-Verlag, New York, pp. 150–174.
- Milton, G. W. (2002). *The Theory of Composites*, Vol. 6 of *Cambridge Monographs on Applied and Computational Mathematics*, Cambridge University Press, New York.
- Milton, G. W. and Kohn, R. V. (1988). Variational bounds on the effective moduli of anisotropic composites, *J. Mech. Phys. Solids* **36**(6): 597–629.
- Nan, C.-W. and Weng, G. J. (2000). Theoretical approach to effective electrostriction in inhomogeneous materials, *Phys. Rev. B* **61**(1): 258–265.
- Ogden, R. W. (1974). On the overall moduli of non-linear elastic composite materials, *J. Mech. Phys. Solids* **22**: 541–553.
- Ogden, R. W. (1997). *Non-Linear Elastic Deformations*, Dover Publications, New York.
- Pelrine, R. E., Kornbluh, R. D. and Joseph, J. P. (1998). Electrostriction of polymer dielectrics with compliant electrodes as a mean of actuation, *Sensors and Actuators A* **64**(1): 77–85.
- Rosen, B. W. and Hashin, Z. (1970). Effective thermal expansion coefficients and specific heats of composite materials, *Int. J. Engng. Sci.* **8**(2): 157–173.
- Socolsky, E. A. (2007). *Electroactive sequentially laminated composites - an exact solution in finite deformation elasticity*, Master's thesis, Ben-Gurion University.
- Sundar, V. and Newnham, R. E. (1992). Electrostriction and polarization, *Ferroelectrics* **135**(1-4): 431–446.
- Tiersten, H. F. (1990). *A Development of the Equations of Electromagnetism in Material Continua*, Vol. 36 of *Springer Tracts in Natural Philosophy*, Springer-Verlag, New York.
- Torquato, S. (1991). Random heterogenous media: microstructure and improved bounds on the effective properties, *Appl. Mech. Rev.* **44**(2): 37–76.
- Torquato, S. and Lado, F. (1992). Improved bounds on the effective elastic moduli of random arrays of cylinders, *J. Appl. Mech., Trans. ASME* **59**(1): 1–6.
- Toupin, R. A. (1956). The elastic dielectric, *Arch. Rational. Mech. Anal.* **5**: 849–915.
- Uchino, K. and Leslie, E. C. (1980). Electrostriction and its interrelation with other anharmonic properties of materials, *Jpn. J. Appl. Phys.* **19**(4): L171–L173.
- Walpole, L. J. (1969). On the overall elastic moduli of composite materials, *J. Mech. Phys. Solids* **17**(4): 235–251.

-
- Walpole, L. J. (1981). Elastic behavior of composite materials: theoretical foundations, *Advances in Applied Mechanics* **21**: 169–242.
- Willis, J. R. (1977). Bounds and self-consistent estimates for the overall properties of anisotropic composites, *J. Mech. Phys. Solids* **25**(3): 185–202.
- Willis, J. R. (1981). Variational and related methods for the overall properties of composites, *Advances in Applied Mechanics* **21**: 1–78.
- Xiao, Y. (2004). *The influence of oxygen vacancies on domain patterns in ferroelectric perovskites*, PhD thesis, California Institute of Technology.
- Xiao, Y. and Bhattacharya, K. (2008). A continuum theory of deformable, semiconducting ferroelectrics, *Archive for Rational Mechanics and Analysis* **189**: 59–95.
- Zhang, Q. M. and Scheinbeim, J. (2001). Electric EAP, in Y. Bar-Cohen (ed.), *Electroactive Polymer (EAP) Actuators as Artificial Muscles*, SPIE press, Bellingham, WA, chapter 4, pp. 89–120.
- Zhang, Q. M., Li, H., Poh, M., Xia, F., Cheng, Z.-Y., Xu, H. and Huang, C. (2002). An all-organic composite actuator material with a high dielectric constant, *Nature* **419**(6904): 284–289.
- Zhao, Y. H. and Weng, G. J. (1990). Effective elastic moduli of ribbon-reinforced composites, *J. Appl. Mech., Trans. ASME* **57**(10): 158–167.

העבודה נעשתה בהדרכת

פרופסור גל דבוטון

במחלקה להנדסת מכונות

בפקולטה להנדסה

פולימרים מרוכבים פעילים מבחינה חשמלית - ניתוח והדמייה

מחקר לשם מיילוי חלקי של הדרישות לקבלת תואר "דוקטור לפילוסופיה"

מאת

לימור טבת-דרעי

הוגש לסינאט אוניברסיטת בן גוריון בנגב

ינואר 2008

שבט תשס"ח

באר שבע

פולימרים מרוכבים פעילים מבחינה חשמלית - ניתוח והדמייה

מחקר לשם מיילוי חלקי של הדרישות לקבלת תואר "דוקטור לפילוסופיה"

מאת

לימור טבת-דרעי

הוגש לסינאט אוניברסיטת בן גוריון בנגב

אישור המנחה _____

אישור דיקן בית הספר ללימודי מחקר מתקדמים ע"ש קרייטמן _____

ינואר 2008

שבט תשס"ח

באר שבע